


# Diagenesis of the Clay-Sulfate Stratigraphic Transition, Mount Sharp Group, Gale Crater, Mars

C. H. Seeger<sup>1</sup>  and J. P. Grotzinger<sup>1</sup><sup>1</sup>Department of Geological and Planetary Sciences, California Institute of Technology, Pasadena, CA, USA**Key Points:**

- The clay-sulfate transition region of Gale crater is marked by significant changes in diversity and abundance of diagenetic textures
- Observed textures and their associated chemistry suggest several diagenetic episodes and concentrations of Mg sulfate in nodules and cement
- We propose several groundwater-based mechanisms to remobilize and precipitate Mg sulfate cement in the subsurface

**Correspondence to:**C. H. Seeger,  
[cseeger@caltech.edu](mailto:cseeger@caltech.edu)**Citation:**Seeger, C. H., & Grotzinger, J. P. (2024). Diagenesis of the clay-sulfate stratigraphic transition, Mount Sharp Group, Gale Crater, Mars. *Journal of Geophysical Research: Planets*, 129, e2024JE008531. <https://doi.org/10.1029/2024JE008531>

Received 24 MAY 2024

Accepted 25 OCT 2024

**Abstract** The diversity and abundance of diagenetic textures observed in sedimentary rocks of the clay-sulfate transition recorded in the stratigraphic record of Gale crater are distinctive within the rover's traverse. This study catalogs all textures observed by the MAHLI instrument, including their abundances, morphologies, and cross-cutting relationships in order to suggest a paragenetic sequence in which multiple episodes of diagenetic fluid flow were required to form co-occurring color variations, pits, and nodules; secondary nodule populations; and two generations of Ca sulfate fracture-filling vein precipitation. Spatial heterogeneities in the abundance and diversity of these textures throughout the studied stratigraphic section loosely correlate with stratigraphic unit, suggesting that grain size and compaction controls on fluid pathways influenced their formation; these patterns are especially prevalent in the Pontours member, where primary stratigraphy is entirely overprinted by a nodular fabric, and the base of the stratigraphic section, where increased textural diversity may be influenced by the underlying less permeable clay-bearing rocks of the Glen Torridon region. Correlations between quantitative nodule abundance and subtle variations in measured bulk rock chemistry (especially MgO and SO<sub>3</sub> enrichment) by the Alpha Particle X-Ray Spectrometer instrument suggest that an increase in Mg sulfate upsection is linked to precipitation of pore-filling diagenetic cement. Due to a lack of sedimentological evidence for widespread evaporite or near-surface crust formation of these Mg sulfates, we propose three alternative hypotheses for subsurface groundwater-related remobilization of pre-existing sulfates and reprecipitation at depth in pore spaces.

**Plain Language Summary** The Curiosity rover on Mars has traversed a ~800 m thick sequence of sedimentary rocks in Gale crater. Recently, the rover has traveled through a region broadly transitioning from wetter environments to drier environments, nominally marked by enrichment in magnesium sulfate, which is so soluble that its presence in the rock record indicates aridification. The rocks in this region contain a wide variety of unique textures—such as color variation, nodules, and veins—created during diagenesis, a formation and modification phase where groundwater flows through pore spaces in the rock after it solidifies. This study catalogs all diagenetic textures observed up-close throughout this region in order to constrain the order in which they formed, and therefore how many episodes of post-formation fluid flow occurred to produce the record that we see. We also compared the nodule abundance in the rocks to their overall elemental chemistry to suggest that the increase in Mg sulfate detected could be concentrated in the nodules and cement. Ultimately, we use the distribution of nodules and other textures to propose three new hypotheses to explain how groundwater could have redistributed these salts in the subsurface, with implications for the timing of Mars aridification.

## 1. Introduction

Sediments and sedimentary rocks on terrestrial bodies can experience multiple generations of transformation, as their constituent grains are transported into a depositional environment, become lithified, and then are subject to subsequent alteration over the course of geologic time—be it aqueous alteration, metamorphism, or weathering. The process of diagenesis, both in cementation and associated mineral authigenesis, and later stage alteration, records a valuable compositional history of the fluids that interact with sediments. This record can come in the form of cement and authigenic mineral assemblages with specific trace element chemistries that reflect specific primary environments or alteration products produced by later-stage fluid movement throughout the rocks (e.g., vein mineral precipitation, nodules, color variations, etc.).

On Earth, understanding diagenesis has helped to deconvolve significant pieces of geologic history. For example, bleaching patterns through the otherwise oxidized red-orange sediments of the Navajo sandstone provide constraints on the chemistry and prevalence of buoyant reducing groundwater fluids (likely hydrocarbons like

© 2024 The Author(s).

This is an open access article under the terms of the [Creative Commons Attribution-NonCommercial License](https://creativecommons.org/licenses/by-nc/4.0/), which permits use, distribution and reproduction in any medium, provided the original work is properly cited and is not used for commercial purposes.

petroleum or methane derived from underlying units) that flowed through heterogeneous pore spaces in these ancient aeolian deposits, moving more easily through the coarser grain flow laminae than the finer-grained, clay-rich wind ripple laminae (e.g., Beitleer et al., 2003, 2005; Bowen et al., 2007; Chan et al., 2000; Parry et al., 2004; Seiler, 2008). These reducing fluids can saturate pore spaces, and when they subsequently come in contact with oxidizing groundwater, diffusion at the interface results in the precipitation of spherical concretions with a distribution determined by geochemical self-organization. Iron oxide concretions in the Navajo sandstone have been widely studied, particularly as analogs for Martian concretions (Beitleer et al., 2005; Chan et al., 2005; Ortoleva, 1993; Potter et al., 2011).

Though water-rock interactions on Mars occur in mafic rather than dominantly felsic sediments, we can still use terrestrial examples and present-day alteration products observed by rovers to understand the chemistry and timing of groundwater fluid flow on Mars, perhaps even after liquid water ceased to exist on the surface. Although far less common, there are terrestrial examples of diagenetic alteration of volcanic sediments, such as the mixed silicic and mafic sediments of the Ochoco basin in Oregon, which experienced diagenesis from the uniform heating of a perched geothermal aquifer under lava flows (Summer & Verosub, 1992). On Earth, diagenesis is often quantified with the water-rock ratio—that is, the mass exchanged between fluid and rock as the fluid passes through and interacts with pore spaces—which can be calculated using stable isotope exchange at equilibrium. Terrestrial equations for volumetric estimates of pore fluids can be modified for Mars with some reasonable assumptions about Martian brines to calculate the amount of diagenetic fluid necessary to produce certain diagenetic features, such as boxwork deposits (e.g., Banner & Hanson, 1990; Siebach & Grotzinger, 2014). Host rock composition can affect the chemical and mineralogical composition of many diagenetic textures, but their physical formation mechanisms are independent of host rock; therefore, terrestrial felsic diagenetic textures remain the most valuable analog for Mars. Previous studies have cataloged diagenetic features in Meridiani Planum, Gusev crater, and Gale crater, as investigated by the Mars Exploration Rover (MER) and Mars Science Laboratory (MSL) Curiosity rover missions (Caswell & Milliken, 2017; Frydenvang et al., 2017; Kah et al., 2018; Kronyak et al., 2019; McLennan et al., 2005; Meyer et al., 2024; Nachon et al., 2014, 2017; Siebach et al., 2014; Stack et al., 2014; Sun et al., 2019; Tosca et al., 2008; Wiens et al., 2017; Yen et al., 2017). These features provide constraints on the chemistry and timing of groundwater movement on Mars, perhaps after liquid water ceased to exist on the surface. In the Murray and Stimson formations in Gale alone, the size, distribution, and paragenetic sequence of the diagenetic textures record at least six post-depositional fluid flow events (Sun et al., 2019).

In this study, we investigate a new suite of diagenetic features exposed in the region of Curiosity's traverse explored from sols 2904–3627, from the Mary Anning drill target in the clay-bearing rocks of the Carolyn Shoemaker formation (Glen Torridon region) to the Canaima drill target in the sulfate-bearing unit of the Mirador formation. Understanding the relationships among these features, and how they relate to host rock chemistry and mineralogy, can constrain the geologic history of groundwater in the subsurface of Gale crater. This has implications for subsurface habitability, and understanding water-rock ratios is an important constraint on limiting habitability as discussed in Knoll and Grotzinger (2006). The Curiosity mission has determined Gale crater to have once been a habitable surface environment (e.g., Grotzinger et al., 2014, 2015; McLennan et al., 2019). It is also worth considering the conditions for subsurface habitability on Mars. Subsurface rock-hosted life has been identified in the terrestrial rock record dating back hundreds of millions of years up to 3.45 Ga (Tice & Lowe, 2004), and modern microbial life is resilient to a wide variety of conditions: microbes have been found up to 5 km in the continental crust (Moser et al., 2005) and 2.5 km in submarine sediments (Inagaki et al., 2015), at temperatures from  $-54^{\circ}\text{C}$  to  $122^{\circ}\text{C}$ , and at pH values from 3 to 13 (Magnabosco et al., 2018). The diversity of environments that support rock-hosted life, from deep groundwater to shallow aquifer and diagenetic fluids, coupled with the early evolution of subsurface life in Earth history and early Martian conditions, support the likely emergence and preservation of similar organisms in a habitable Martian subsurface (Onstott et al., 2019). Indeed, there is chemical evidence that diagenetic fluids precipitating cement in subsurface fractures that weathered into distinctive early vein filling cement in Gale crater's Sheepbed mudstone were potentially habitable, with a low salinity to brackish composition at near-neutral or slightly alkaline pH (Léveillé et al., 2014). By using diagenetic features to explore the ways subsurface fluids may have interacted with basaltic sediments—a process that on Earth is known to sustain life—we may be able to expand the time and conditions under which life could have existed on Mars.

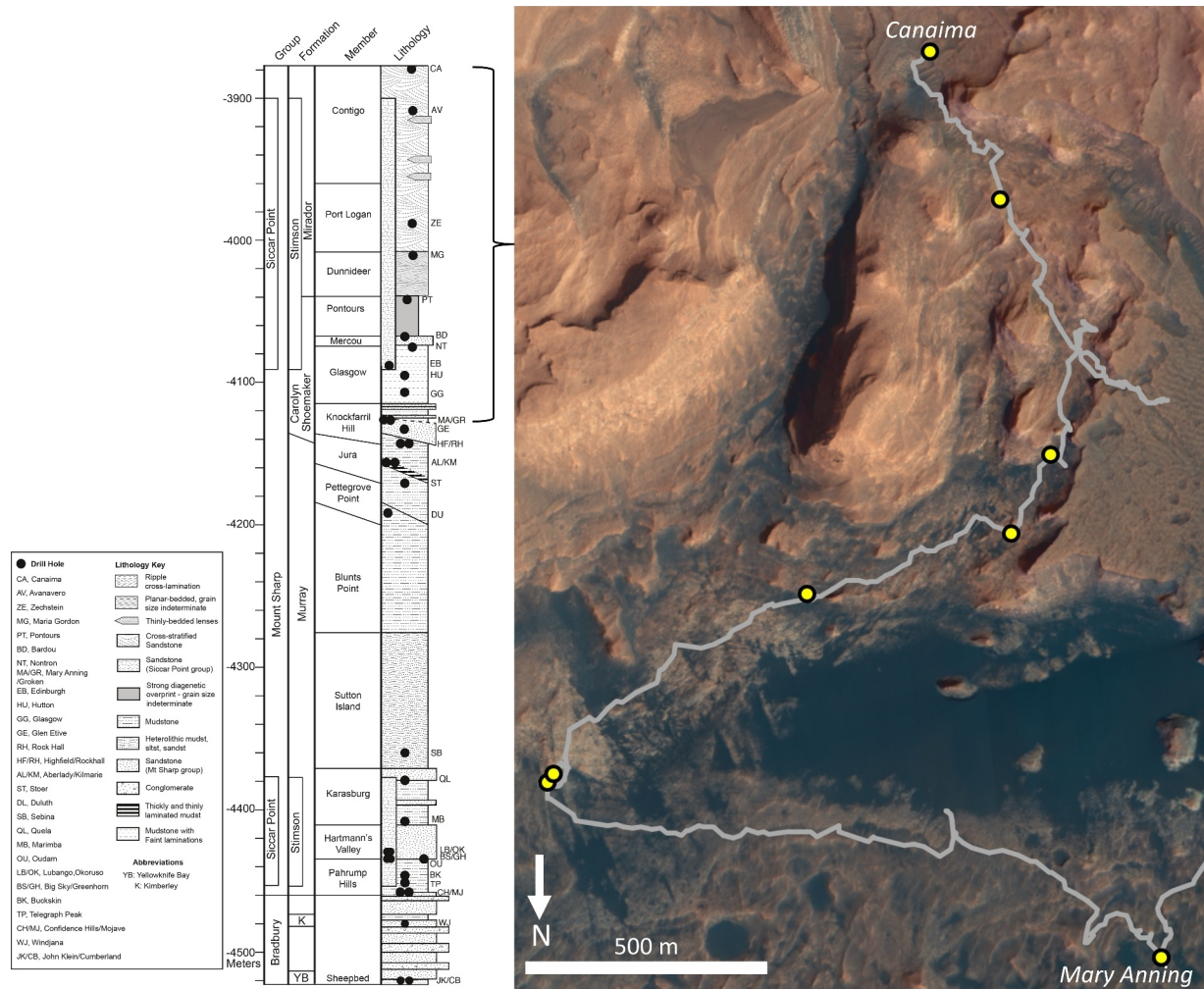


**Figure 1.** Stratigraphic and geographic context for Curiosity's traverse through the study region in Gale crater, with drill targets mapped as yellow circles. This schematic stratigraphic column is a summary of the geology encountered along a lateral traverse through Gale crater condensed into a representative vertical section, with the formations and members referred to in this study outlined at the top.

## 2. Geologic Context

The Mars Science Laboratory team, using the Curiosity rover, has spent the last twelve years exploring Gale crater, a ~150 km diameter impact crater located along the Martian crustal dichotomy boundary that is interpreted to have formed ~3.6–3.8 Ga (Le Deit et al., 2013; Thomson et al., 2011) (Figure 1). This landing site was selected based on the vast sedimentary record exposed along the crater's large, ~5 km tall central mound (Aeolis Mons or, informally, Mount Sharp) that contained distinctive spectral signatures detected from orbit as well as geomorphic signatures of past aqueous events (Anderson and Bell, 2010; Fraeman et al., 2013; Grotzinger et al., 2014; Le Deit et al., 2013; Milliken et al., 2010; Thomson et al., 2011). The rocks exposed along the lower slopes of Mount Sharp are broadly divisible into two units based on their spectral absorptions detected by the Compact Reconnaissance Imaging Spectrometer for Mars (CRISM) instrument: a lower unit that contains hydrated signatures consistent with clay-bearing minerals like nontronite, mixed sulfates and smectites, and Mg-bearing sulfates like kieserite; and an upper unit marked by anhydrous iron oxide spectra (Milliken et al., 2010; Sheppard et al., 2021; Thomson et al., 2011). These two units are separated by an erosional unconformity, which was first recognized by Malin and Edgett (2000) and provides the broadest subdivision of Mount Sharp stratigraphy into hydrated lower and anhydrous upper sediments. The lower unit is divisible into three members, where the transition between phyllosilicate-bearing strata into sulfate-bearing strata occurs within the middle member. This transition is

broadly suggestive of a large environmental shift from a wet to dry environment, consistent with the global aridification of Mars (Milliken et al., 2010).

Orbital studies complement the in situ observations and measurements made by the rovers on the ground. These two observational scales, taken together, give a more complete picture of geologic history than either can independently; rover data can provide textural and compositional details in specific locations, which can then be related to spectral signatures and visual imagery that extend far beyond the rover's limited footprint on the ground. Over the past ten years, Curiosity has traveled 32 km along the floor of Gale crater, and then up the side of Mount Sharp, gaining over 800 m of elevation. Because the strata composing Mount Sharp are relatively flat lying, this ascent of Mount Sharp, despite some lateral variability, can be represented by a generalized stratigraphic column as seen by the rover's ascent through the ~800 m of strata (Figure 1).

From the landing site near Yellowknife Bay, Curiosity traversed through the fluvio-deltaic sediments of the Bradbury group before reaching the lacustrine mudstones of the Murray formation at the foothills of Mount Sharp (Fraeman et al., 2020; Grotzinger et al., 2015; Hurowitz et al., 2017; Rampe et al., 2017; Williams et al., 2013). The 300-m-thick package of lacustrine deposits was dominantly planar laminated very fine grained sandstone and mudstone and contained veins and nodules indicative of late stage diagenetic alteration (Fedo et al., 2022; Kronyak et al., 2019; Rivera-Hernández et al., 2020; Sun et al., 2019). The Murray formation gave way to the overlying lacustrine and fluvial strata of the clay-rich Carolyn Shoemaker formation, marking a major paleo-environmental shift to a marginal lake environment (Caravaca et al., 2022; Cardenas et al., 2022; Fedo et al., 2022), which was eventually succeeded by an aeolian environment marked by large-scale cross-stratified sandstones of the Mirador formation (Edgar et al., 2024; Meyer et al., 2024).

The Murray and Carolyn Shoemaker formations are consistent with the strata recognized from orbit to be clay-bearing, while the Mirador formation straddles the transition into the Mg sulfate-bearing unit. Therefore, this study focuses on rover observations from sols 2904–3627, which span the transition of ~250 m of stratigraphy from clays to Mg sulfates, from –4,127 to –3,879 m (Figure 1). The need to circumnavigate a modern eolian sand deposit resulted in a long (1–1.5 km each way) lateral traverse through much of this section, which provided the opportunity to analyze along-strike spatial heterogeneities in this unit, particularly in terms of diagenetic feature diversity, which increased significantly throughout this unit. This lateral traverse through the Glasgow member of the Carolyn Shoemaker formation led Fedo et al. (2022) to characterize the gray mudstone with millimeter-scale lamination as lacustrine deposits, though Cardenas et al. (2022) identified topographic benches at the eastern end of the traverse to be point-bar deposits or deltaic mouth bars. A ~7-m-tall cliff feature named Mont Mercou contains strata with variable dip directions consistent with a downstream-migrating fluvial barform that, along with a neighboring ridge, is part of a partially exposed channel belt (Cardenas et al., 2022). Though a wider regional rover exploration would be needed to determine if these barforms are simply the result of river avulsion, it is likely that the fluvial progradation of the Glasgow and Mercou members over the lacustrine Murray formation strata records the shrinking of the Gale lake system in a drying climate. Approximately 25 m above Mont Mercou, at the Carolyn Shoemaker—Mirador formation boundary, these fluvial strata gave way to large scale cross bedded aeolian sandstones with occasional wave ripple-laminated lenses, further solidifying this interpretation as an environmental shift (Edgar et al., 2024).

### 3. Methods

This study utilized close-up image data collected by the Mars Hand Lens Imager (MAHLI) and contextualized by Mast Camera (Mastcam) imagery, and compositional data collected by the Alpha Particle X-Ray Spectrometer (APXS) that was supplemented by the ChemCam, CheMin, and SAM instruments. The Mastcam instrument consists of two cameras (focal lengths of 34 mm (M34) and 100 mm (M100)) that together capture stereo imagery of nearfield (“workspace” right in front of the rover) and more distant targets (Bell et al., 2017; Malin et al., 2017). Along the study area, Mastcam workspace and drive direction images were analyzed to understand the distribution of diagenetic features (particularly nodules) within the strata. With an M100 resolution of ~150  $\mu\text{m}/\text{pixel}$  for targets 2 m away, these images were most useful in identifying large, cm-scale nodules, but were not sufficient for the pervasive smaller nodules along the traverse. However, this imagery was essential to document nodules occurring in patches or organized patterns, particularly when they appeared at a distance from where the rover was parked.

Detailed documentation and analysis of the diagenetic features was performed and compiled into a database (Seeger & Grotzinger, 2024) using imagery from the up-close MAHLI imager located on the rover's arm (Edgett et al., 2012). These images were taken at a variety of standoff distances from the rock surface (25 cm, 5 cm, and occasional closer standoffs), with an average resolution of 100 microns/pixel for high standoff and 30 microns/pixel for closer standoff (Edgett et al., 2012). This study utilized 284 MAHLI targets, supplemented with Mastcam imagery during short periods when the MAHLI instrument was offline. Observations based on MAHLI imagery comprise the bulk of the database of diagenetic features used for this study, as the high resolution, up-close imagery was necessary to resolve the size and shape of many of the millimeter-scale nodules encountered (Seeger & Grotzinger, 2024). In a subset of MAHLI images, individual diagenetic nodules were traced in order to create a binary mask that could be analyzed via a Python script to quantify nodule abundance. This analysis was restricted to the circular area brushed by the Dust Removal Tool (DRT) within each MAHLI image for consistency with other instrument data sets. We therefore determine the percentage of areal coverage by nodules (independent of their clustering or distribution across the outcrop) by calculating the number of pixels associated with a nodule divided by the total number of pixels in the field of view, including host rock (Figure 4). Abundance measurements are a lower limit due to the nature of tracing nodules at such a small scale; shadows, image resolution, and dust distribution (particularly in brushed spots) can obscure the true size and shape of some nodules; therefore, those that could not be definitively identified were omitted from measurements.

We relate diagenetic feature abundance to host rock chemistry using elemental abundances derived from the APXS instrument measurements within a 1.7 cm diameter sampled area (Campbell et al., 2012). APXS emits X-rays and alpha particles, and measures the resultant characteristic energy emitted by the constituent elements in the rock to determine the elemental composition. There were 218 APXS measurements on 131 targets collected within the study area, 85 of which were on 46 targets cleared of dust with the Dust Removal Tool (DRT) that had concurrent MAHLI imaging (Berger, 2024). Previous studies have linked populations of nodules to variations in elemental composition using ChemCam observations, which can discern individual nodules from host rock due to the instrument's ~200–400  $\mu\text{m}$  diameter laser spot size used to detect elemental abundances via laser-induced breakdown spectroscopy (Meyer et al., 2024; Wiens et al., 2012). From this work, we derive the elements most closely associated with the nodular features to be Mg, S, and Fe. By correlating APXS bulk rock elemental composition, which is a mixture of nodule and host rock, with the quantitative abundances of the nodules as measured in MAHLI imagery, we provide new context for how these unique diagenetic features contribute to bulk rock chemistry. However, these correlations are only general, as there are limitations to this approach: the APXS instrument has radial sensitivity in which 50% of the spectrum comes from the innermost 16% of the field of view (VanBommel et al., 2016), so the elemental contribution from nodules is highly dependent on the location of a nodule in the center of the field of view. The calculated nodule abundances are representative of the rock as a whole, but a deconvolution using several APXS rasters for each point would be necessary to precisely reflect the contribution from specific nodules to draw more precise conclusions (VanBommel et al., 2016, 2017).

In addition to the elemental data distributed across the study area, ten drill holes were also analyzed for their mineralogic composition by the Chemistry and Mineralogy (CheMin) X-ray diffractometer, which uses the characteristic X-ray diffraction patterns and fluorescence emitted by specific atoms and crystal structures to identify the minerals within the sample (Blake et al., 2012; Downs et al., 2015). These drilled samples provide bulk rock composition, which enables identification of major and minor minerals and phases in the host rock, and sometimes includes diagenetic features in the near-subsurface.

#### 4. Facies Descriptions of Diagenetic Features

A variety of diagenetic features has been documented in abundance throughout Curiosity's traverse (e.g., Gasda et al., 2022; Grotzinger et al., 2014; Meyer et al., 2024; Siebach et al., 2014; Stack et al., 2014; Sun et al., 2019). In the study area of the clay-sulfate transition region, a broad range of fabric elements became abundant in the rocks. Previous work has documented the fine-scale chemistry and variability of some of these textures—particularly nodules—using the ChemCam instrument (Meyer et al., 2024). This complementary study includes a detailed characterization of the breadth of features observed (including nodules and their morphology) from a complementary perspective, using the high-resolution imagery of the MAHLI instrument and relationships to broader bulk rock chemistry to further illuminate the relationship between diagenetic textures, primary stratigraphy, and groundwater history in this region.

#### 4.1. Pits and Color Variations

Pits are negative relief, circular features embedded within the mudstones of the Carolyn Shoemaker formation (Figure 2a). They are sub-millimeter in diameter, and often co-occur with color variations in the rock. The grain size of the enclosing matrix rock is below the resolution of MAHLI (therefore, finer than very fine sand), so these do not appear to be void casts of sand grains that have weathered out. Zones of color variation appear as centimeter-scale irregularly bounded redder-tone splotches that are otherwise texturally indistinguishable from the rest of the rock (Figure 2a). In the Sol 3110 target Gourdon, the rover's wheels broke some rocks revealing color variations in three dimensions on a fresh face, indicating that this alteration pattern is consistent through several centimeters below the surface at minimum (Figure 2b).

Terrestrial sandstones frequently exhibit zones of color variation independent of any changes in chemical composition; for example, the Navajo sandstone has both splotchy and layered zones of whiter sediments than their oxidized red counterparts due to fronts of reducing fluids interacting with the iron oxides that converted ferric iron to ferrous iron (e.g., Beitler et al., 2003). We infer that a similar diagenetic event or events contributed to the color variations observed in the Martian outcrops. It is possible that the pits are dissolution features created by undersaturated fluids moving through pore spaces—perhaps the same fluids that caused zones of color variation, as the two features often co-occur.

#### 4.2. Pervasive Concentric Fabric

The upper Glasgow member of the Carolyn Shoemaker formation contains several occurrences of a pervasive concentric fabric in some outcrops, composed of millimeter- to centimeter-scale circles of white rock that sometimes have cores or concentric rings of different colors (Figure 2c). When developed, these features occur in such abundance that they dominate the entire surface of the rock. There is no relief difference associated with this fabric, and it otherwise has an identical texture to the surrounding rock.

#### 4.3. Small Dark Subangular Nodules

In two localities, there are highly abundant small dark subangular nodules that approximately adhere to bedding planes and extend in patches up to ~10 cm across (Figure 2d). These features, seen at targets Groken and Pezuls, have a distinctive elemental composition (high in manganese and phosphorous) and have been the subject of detailed investigation (Treiman et al., 2023; VanBommel et al., 2023). These millimeter-scale dark features are very abundant on the individual bedding planes on which they are exposed. There are no examples of sediment draping over them to indicate syndepositional formation; therefore, they likely precipitated from diagenetic fluids flowing along differently compacted bedding planes after lithification.

#### 4.4. Veins and Fins

Calcium-sulfate veins have been observed consistently across all stratigraphic units of Gale crater, from Yellownknife Bay to the mudstones of the Murray formation, and—to a much lesser extent—the unconformably overlying aeolian sandstones of the Stimson formation (Caswell & Milliken, 2017; Kronyak et al., 2019; Nachon et al., 2017; Sun et al., 2019). They are present in every member of the stratigraphic section of this study, though they do vary in quantity; their occurrence is therefore only recorded in this survey for outcrops where they are a dominant feature occurring in abundance. Vein fills also appear as flat, high-relief, sometimes layered surfaces described as fins (Figures 2e and 2f). These veins are a result of mineral precipitation in structural rock fractures, and are invariably filled with calcium-sulfate precipitate, though local enrichment in iron and magnesium provide important metrics to understand the variability in groundwater redox chemistry and pH conditions (L'Haridon et al., 2018). Fins in this study area are compositionally similar to veins, and less similar to the dark-toned fin-like veins encountered in the Murray formation (Kronyak et al., 2019). Because these features are so pervasive as late-stage diagenetic features (cross-cutting bedding and some earlier generations of veins), they are an essential component of the regional diagenetic history.

#### 4.5. Irregular Raised and Rounded Nodules

Perhaps the most abundant diagenetic features are irregularly shaped, dark-toned, high relief nodules. They range from sub-millimeter scale to several centimeters in diameter but exhibit similar morphologies across all scales so

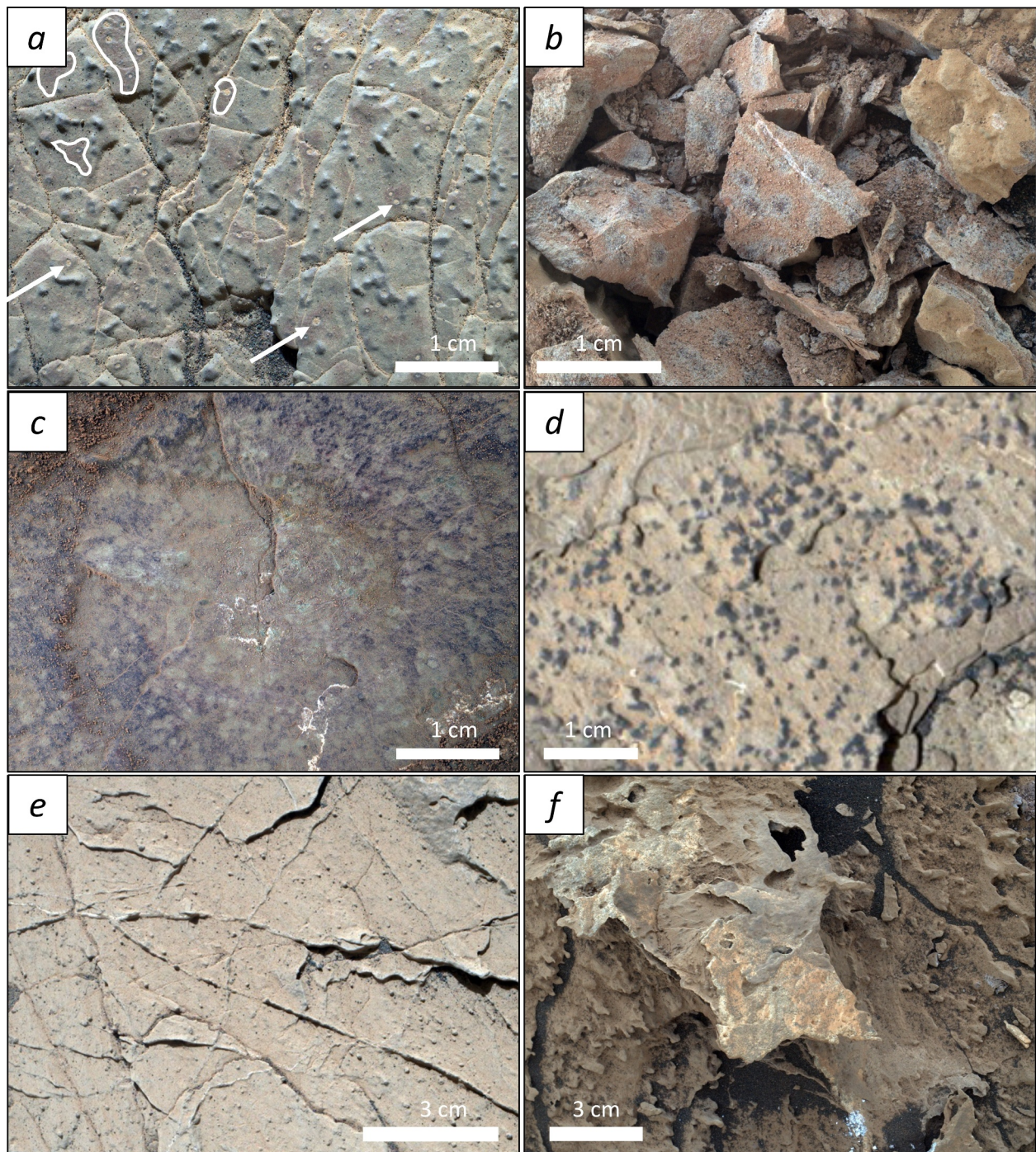


**Figure 2.** Type examples of the array of diagenetic features encountered throughout the clay-sulfate transition region. (a) Color variations, pits, and raised nodules in Sol 3004 target Tomb of the Eagles from MAHLI image 3005MH0001930001100120R00. Example red color splotches are outlined in white and example dust-filled pits are highlighted by white arrows; (b) Fresh rock face broken by rover's wheels exhibiting color variations in three dimensions, Sol 3110 target Gourdon from MAHLI image 3110MH0001930001101741R00; (c) Pervasive concentric fabric in Sol 3024 target Coutures from MAHLI image 3025MH0001630001100520R00; (d) Small dark subangular features from Sol 2906 target Groken in MAHLI image 2906MH0004240011003481C00; (e) Light-toned Ca-sulfate veins from Sol 3054 target Nontron in MAHLI image 3054MH0001900011101097C00; (f) High relief fin-type veins from Sol 3112 target Pezuls in MAHLI image 3112MH0007060021101749C00.

are documented and described as a single group (Figures 3a–3c). For a further subdivision of these nodules into classes based on color, size, and composition, see Meyer et al. (2024). Thirteen percent of the examined outcrops containing these nodules have two size populations co-occurring within any given outcrop (Seeger & Grotzinger, 2024). While there are some notable shape-based populations, such as the spherical nodules just above the Zechstein drill hole (which are very round, but not as perfect or as chemically ferric as the hematite “blueberries” in Meridiani Planum (e.g., McLennan et al., 2005)), most can be described as rounded, isolated nodules that sometimes amalgamate into vermiform chains or larger popcorn-like features (Figure 3b). Indeed, MAHLI imagery of many of the large nodules visible in Mastcam imagery shows that they may be composed of smaller nodules coalescing together. These nodules sometimes occur in centimeter- to decimeter-wide patches, and other times completely dominate an outcrop (Figure 3d). Where primary stratification is visible, the nodules cross-cut lamination and are not concentrated within certain bedding planes like the small dark subangular nodules. Though Meyer et al. (2024) define a class of lamination-enhancing mm-scale nodules based on ChemCam Remote Micro-Imager (RMI) images, we do not observe a similar distribution in the closer-up MAHLI images aside from rare cases; instead, the mm and sub-mm populations of nodules are distributed across the entire outcrop face. Data collection might influence this discrepancy; MAHLI images are most often taken on smooth, flat-topped rock surfaces due to engineering constraints with associated DRT brushes and APXS measurements, while ChemCam measurements can be taken on more vertically layered surfaces farther from the rover. In some instances, throughgoing lamination can be traced within some larger nodules (e.g. sol 3605 MAHLI target “Tapirapeco” and Meyer et al., 2024, Figure 9A and I). Nodule abundance often anticorrelates with visible primary stratification, and there are notable outcrops of palimpsest lamination (Edgar et al., 2024) as well as regions where the primary bedding is entirely overprinted by nodules (Figure 3d).

In some instances, clusters of nodules are arranged into distinctive patterns. In one locality (Sol 3170 Mastcam mosaic mcam00383), nodules are grouped at the edges of exposed bedding planes, with dendrite-like growth patterns visible in cross-section where it appears minerals could have precipitated to form structures with a growth direction perpendicular to bedding (Figure 3e). There are also multiple regions with nodules arranged in a chevron pattern, where chains of amalgamated nodules stand in centimeter-scale relief above the bedrock, arranged into evenly spaced ~2 cm wide rows that zigzag across meter-scale regions of flay-lying bedrock (Figure 3f). These features may be related to a similar raised-ridge polygonal features encountered ~10 stratigraphic meters above the chevron pattern. The raised boundaries of the polygons have the same amalgamated nodular texture as the chevron pattern, and their spacing is slightly bigger at ~5 cm in diameter (Figure 3g). These polygonal features may be related to desiccation features (Rapin et al., 2023) or alternatively were the result of self-organized reaction fronts as the diagenetic fluids moved through pore spaces in these rocks (e.g., Ortoleva, 1993). All of these organized nodule patterns were observed within 25 vertical meters of the Pontours drill target, where diagenetic textures pervasively overprint and obscure primary stratification, and at the boundary of a major facies transition from the aqueously deposited Carolyn Shoemaker formation to the aeolian Mirador formation (Edgar et al., 2024). This spatial relationship indicates that a large volume of fluid moved through pore spaces unevenly; perhaps it was a larger volume of fluid than elsewhere, and this resulted in more reaction-front style movement.

## 5. Relationships Between Diagenetic Features

### 5.1. Nodule Spacing and Size

Using pixel-by-pixel abundance calculations, we are able to quantify the abundance of nodules in any given bedrock target. Here, we focus on 22 representative nodular targets that were also analyzed by APXS in order to correlate variations in elemental composition with nodule abundance. By creating a binary mask over each MAHLI image demarcating nodules from host rock, we can calculate their abundance, size distribution, and spacing (Figure 4). The densest population of nodules measured corresponds to 25% by area (usually the size of the brushed spot), while the sparsest occurrences of nodules only populate 1.3% of the masked field of view. We have classified nodular outcrops into three categories: sparse (1%–9% nodules by area), moderate (10%–19%), and dense (>20%), and used these classifications to better understand the subtle chemical variations in otherwise consistent bulk rock chemistry throughout the clay-sulfate transition (Figures 5 and 6).

Because nodule formation is limited by pore fluid saturation levels, we can use these abundances and spacings to understand the timing and number of events where fluids move through the rock. Most occurrences of nodules have a dominant size, but there are 24 targets containing two populations of tiny (mm-scale) and large (cm-scale)



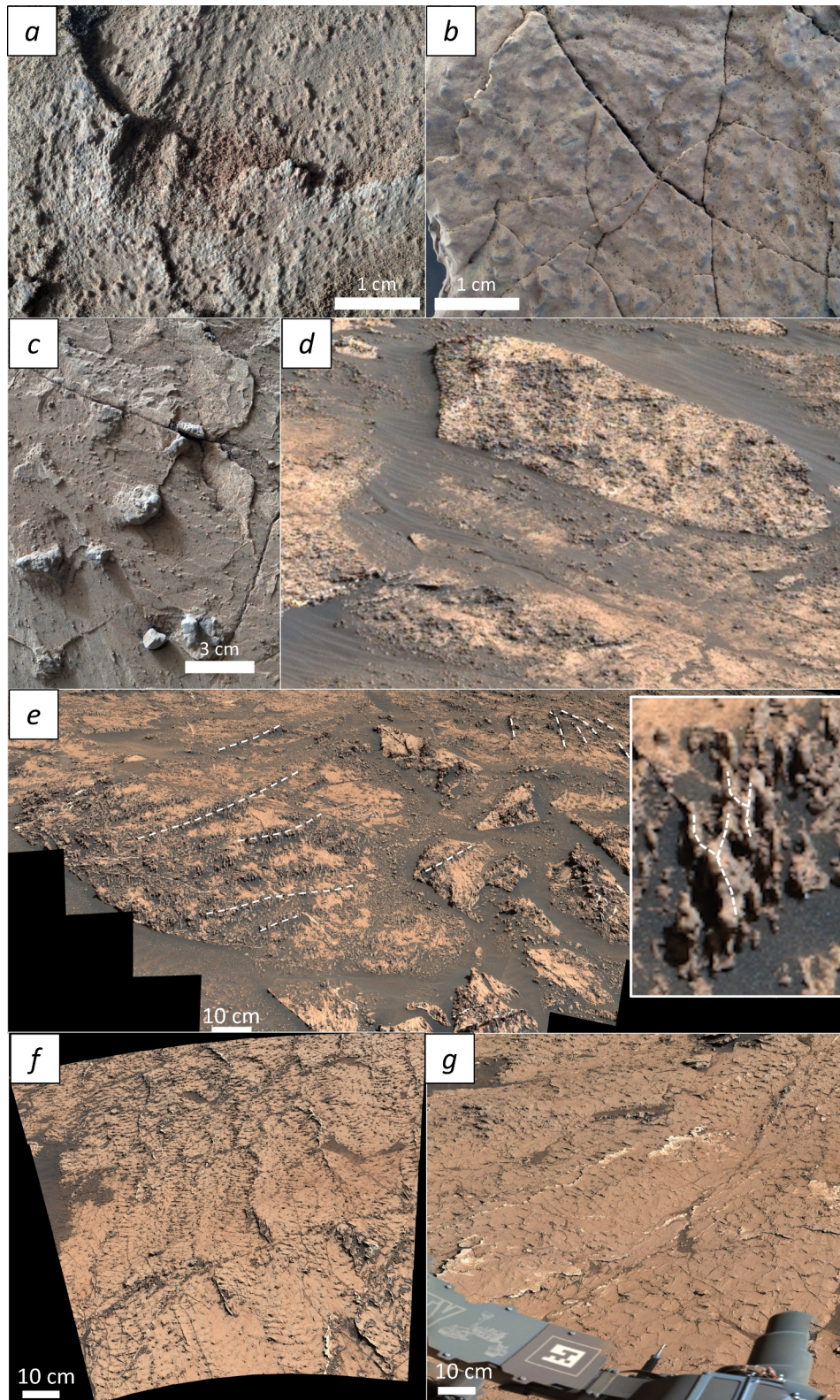


Figure 3.

nodule sizes, with all but two examples occurring stratigraphically above the Pontours drill site, distributed throughout the Mirador formation (Seeger & Grotzinger, 2024). For example, in the sol 3194 target Bregout, ~1 mm nodules are pervasive and overprint some of the larger nodules. Their similarity in morphology to the larger, more amalgamated nodules suggests they may be the result of a remobilization of fluids with similar elemental composition but under slightly different conditions, such as lower permeability, limiting fluid penetration and therefore causing precipitation of smaller features during any given fluid infiltration or reaction event. In localities where multiple populations of nodules co-occur, several explanations are possible: variations in porosity and proximity to fluid front may have allowed cementing crystals to grow larger in some areas than others, or multiple generations of cementation could have assisted some nodules in growing larger than others over time.

We also compared nodule distribution to the nearest-neighbor statistics computed for nodule analysis of the Burns formation at Meridiani Planum (McLennan et al., 2005). Though the Burns formation is composed of dominantly sulfate-cemented basaltic sand deposited in an aeolian environment, the diagenetic nodules found within are a well-studied analog to compare to the nodules of this study (Grotzinger et al., 2005; McLennan et al., 2005; Squyres et al., 2004). The spherical nodules at Meridiani do not follow a random distribution, and at small separation distances suggest that nucleation at one site precludes the nucleation of another nodule within a certain radius due to locally depleted solute. Rare “doublets” and “triplets” contradict this model, indicating that local heterogeneities in porosity and permeability create zones of enriched or depleted solute. The abundance of chain-linked and amalgamated nodule clusters in the Gale data set therefore aligns more with the small-scale heterogeneity model than the radial exclusion zone of the dominantly singular Meridiani nodules. However, perhaps more likely than a radial exclusion zone is a lateral exclusion zone orthogonal to the direction of fluid propagation, creating the clustering and chain-like arrangement of nodules aligned in a given direction. While this phenomenon may be most obvious in the large-scale chevron and polygonal patterns created by nodule chains, it may also be observed in nodule-scale subtle alignment patterns such as the general upper left to lower right fabric visible in Figure 4b (though this could possibly be the result of incidence angle bias).

## 5.2. Cross-Cutting Relationships

Determining the paragenetic sequence of diagenetic textures helps constrain the nature and timing of post-depositional subsurface fluid flow events. For every texture, there is at least one instance of co-occurrence with another texture type. For example, veins, which have been observed consistently throughout Gale crater, often bisect other textures. Though it is not common to observe veins cutting singular nodules, partly due to probability, they do obviously cross-cut high-standing large cluster-like nodules. This is particularly evident in areas of meter-scale surface expression of nodule organization into linear, polygon, or chevron shapes, where large veins intersect large swaths of the nodule pattern (Figure 3). However, the cross-cutting relationships are not uniformly obvious, and these relationships can be obscured by irregular shapes, dust cover, and multiple generations of feature formation (e.g., high-angle fractures cut across low-angle fractures that often parallel and sometimes obscure bedding planes).

A subtle and poorly expressed but very distinctive cm-scale vertical fabric is evident in several nodular outcrops, including the upper 2/3 of outcrop expressed at Mont Mercou. This fabric is defined by long, straight, parallel columns a few centimeters in width that are spaced approximately ten cm apart and can be traced vertically for one or more meters (Figure 7). The texture within the columns is subtle, but is slightly more resistant to erosion and slightly obscures the primary stratification. This fabric is cross-cut by the more defined fractures through the upper portion of the outcrop (Mondro et al., 2023), which further complicates our interpretation of the paragenetic sequence; perhaps this verticality is created by fluids exploiting zones of weakness that later develop into fractures.

**Figure 3.** Type examples of nodular features encountered in bedrock, demonstrating the diversity of their expressions. (a) Sub-millimeter scale nodules visible in DRT spot of Sol 3205 target Grimshader in MALHI image 3206MH0002270001102997R00; (b) ~5 mm nodules, arranged independently and in some linear and some vermiform chains, Sol 3024 target Biron in MALHI image 3025MH0001630001100514R00; (c) large ~2 cm nodules in Sol 3051 target Peyrat in MALHI image 3051MH0007060021101063C00; (d) Example of high nodule abundance overprinting and erasing primary stratification, Sol 03202 Mastcam image mcam100573; (e) linearly organized nodules with dendritic growth pattern (inset), Sol 3170 Mastcam image mcam00383; (f) Chevron pattern in Sol 3139 workspace, Mastcam image mcam00178; (g) Polygonal pattern in Sol 3154 workspace, Mastcam image mcam00270.

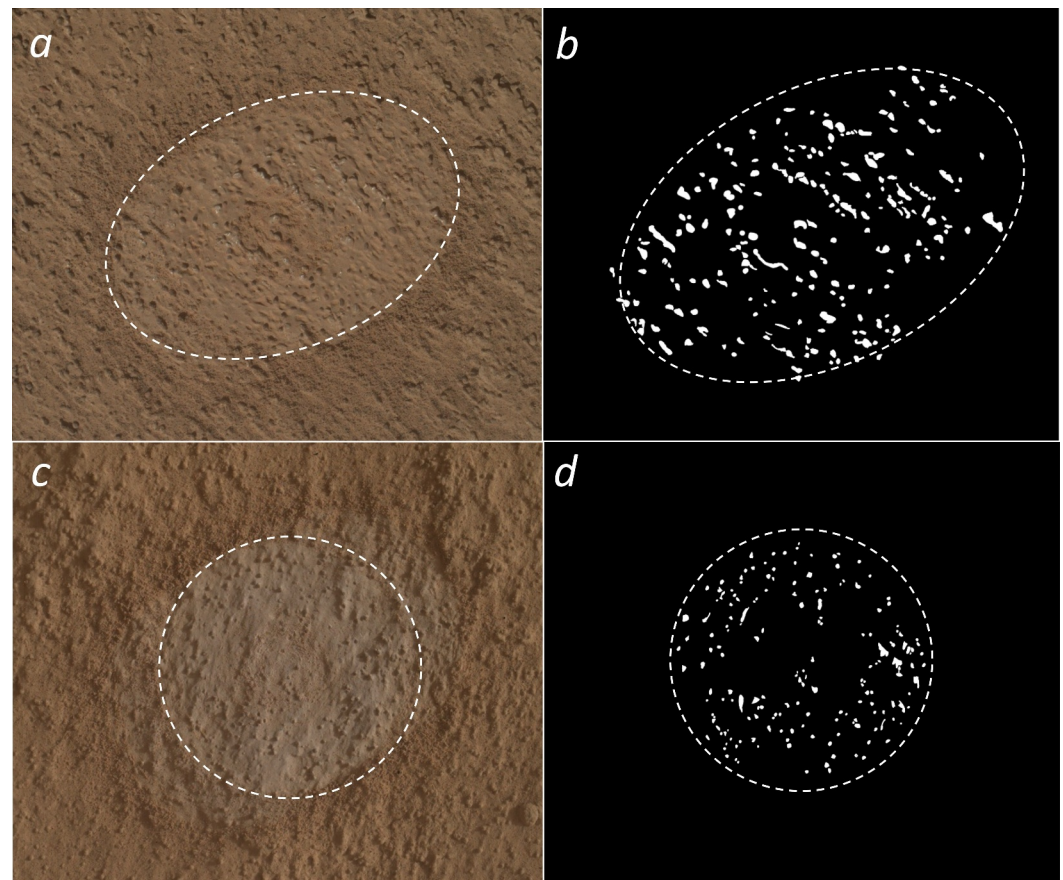


**Figure 4.** Image processing techniques were used to better quantify nodule abundance, especially in targets that were analyzed for elemental composition with APXS. (a) Outlined DRT spot in sol 3224 target Maria Gordon with (b) corresponding binary image mask distinguishing nodules (white) from bedrock (black). (c) Outlined DRT spot in sol 3388 target Loch Coriusk with (d) corresponding binary image mask distinguishing nodules (white) from bedrock (black). DRT spots are  $\sim 4.5$  cm wide.

The fractures, vein fills, and spaced vertical fabric are considered late-stage diagenesis, but it cannot be discounted that some nodule formation—particularly the subvertical chain pattern—could have also occurred later than some other nodule formation. The estimated paragenetic sequence for all diagenetic feature types observed in the study area is summarized in Figure 8, where color variation, pit, and nodule formation cannot be disentangled but form sometime after lithification. Because nodules and color variations do not overprint one another, they may have formed under the same conditions, where small heterogeneous variations in pore space (possibly due to compaction) resulted in leaching from some areas and precipitation in others. Bimodal nodule size populations and the organization of some nodules into larger clusters or organized chains suggest at least two different diagenetic events. The latest stage of alteration includes at least two generations of fracturing followed by Ca sulfate vein precipitation, first in a subhorizontal orientation, and later forming high-angle fracture-filling veins.

### 5.3. Feature Distribution Along Rover Traverse

The diverse array of diagenetic textures encountered along Curiosity's traverse allows us to track fluid movement through different parts of the Gale sedimentary basin, as recorded by its stratigraphic record. Figures 5 and 6 summarize the distribution of these features. Due to the nature of the rover's route, a large lateral traverse—mostly along strike—of the  $\sim 40$  m thick Glasgow member of the Carolyn Shoemaker formation was sampled. From the Mary Anning drill site to Mont Mercou, diagenetic textures increased dramatically in abundance and diversity, but did not overprint bedding; rather, unique textures (such as color variations and pervasive concentric fabric)

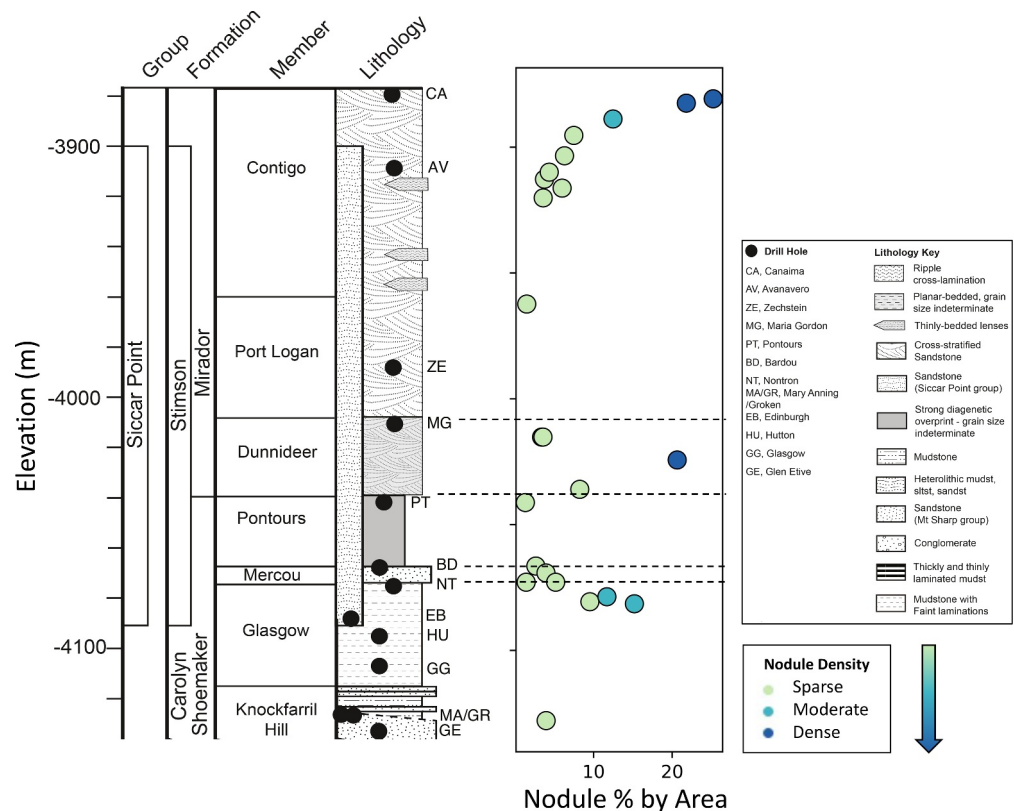


**Figure 5.** Distribution of nodule abundances (% by area) across clay-sulfate transition region for APXS targets where elemental data was collected; dot color corresponds to abundance characterizations of sparse (1%–9% nodules by area), moderate (10%–19%), and dense (>20%) nodules.

were observed but did not alter the host rock to a degree greater than that previously observed in the mission (Sun et al., 2019). The Mont Mercou locality marked a distinct shift in the expression of diagenetic overprints; though the drill holes at the base of the cliff (Nontron) and on top of the cliff (Bardou) have very similar elemental compositions (Rampe et al., 2022), strong overprinting of primary stratification at the base becomes amplified in the upper third of the vertical outcrop, where primary stratification is completely destroyed (Figure 7). This overprint consists of low-angle fractures, nodules, veins, and the subtle centimeter-scale vertical fabric described above. Cardenas et al. (2022) interpret the erosion-resistant strata of Mont Mercou to be a downstream-migrating fluvial barform that is part of a larger channel belt, indicating that this outcrop not only marks a shift in diagenetic alteration but also a shift in depositional environment during lake level in the gradual drying of the Gale lacustrine system. The change in grain size (and therefore porosity) in this barform could have increased pathways for a fluid front to move through the sediments and overprint primary strata to a significant extent uncommon in Gale crater, resulting in a total loss of primary stratification in some zones.

Moving up stratigraphically from Mont Mercou, nodules and veins dominate the strata, and pervasively overprint and erase primary stratification. At the Pontours drill site, just below a transition into low-angle cross-stratified sandstones, nodules are extremely abundant and primary stratification is completely overprinted. The examples of outcrop-scale nodule organization into chevrons and polygonal shapes are also concentrated in the ~25 m of stratigraphy below this drill hole. The presence of nodules remains strong from Pontours to Maria Gordon, though cross-stratification is interspersed with several-meter-scale patches of large, irregular and rounded centimeter-scale nodules (Edgar et al., 2024). Above Maria Gordon, nodules are smaller, sparser, and less obstructive of the primary large-scale cross-stratification (Edgar et al., 2024), though there are some notable variations: just above the Zechstein drill hole, highly spherical nodules are abundant. These have similar elemental composition and morphology to the raised and rounded nodules observed at lower stratigraphic levels, and therefore differ from the hematite “blueberries” in the Burns formation at Meridiani planum. Additionally, in the same area, there

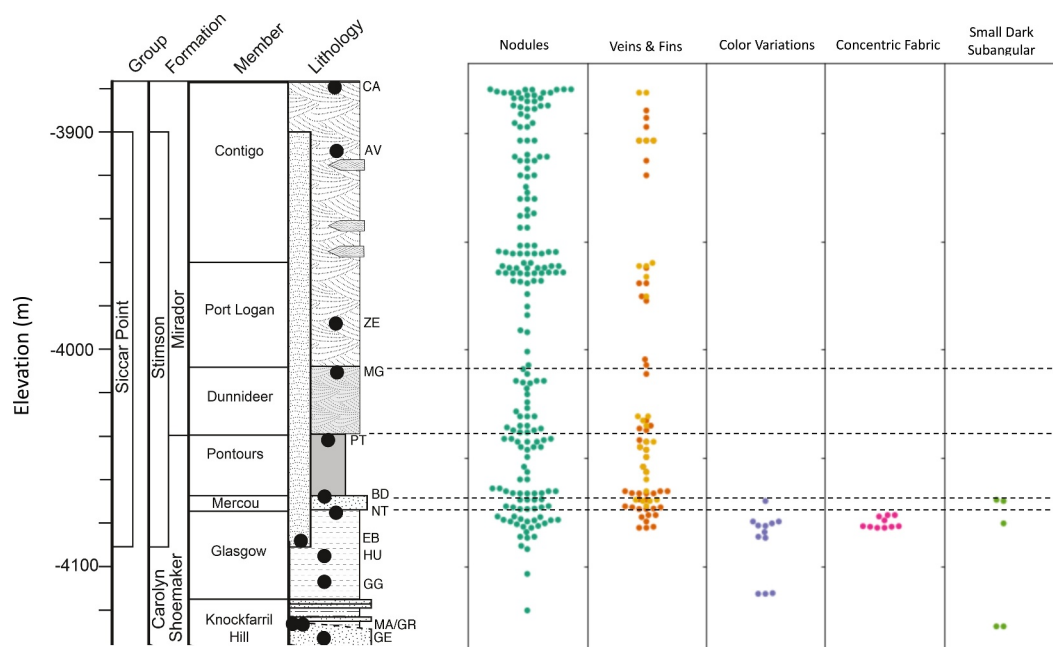


**Figure 6.** A schematic stratigraphic column corresponds to a simplified representation of rock units encountered along a lateral traverse condensed into a representative vertical section; locations where each diagenetic feature type was observed are marked by elevation to correspond with stratigraphic units. Note that veins are ubiquitous in Gale crater but only recorded here in outcrops where they are an abundant, dominant feature.

are centimeter-scale highly angular nodules that appear to be concentrated along bedding planes. Due to image resolution and the angles at which these features are exposed, we cannot conclusively determine if they are pseudomorphs after evaporite hopper crystals (e.g., halite), but the possibility of very late stage evaporite deposits in resurgent brines could be considered.



**Figure 7.** Vertical exposure of Mont Mercou outcrop demonstrating subtle vertical fabric independent of fracturing; three regions with resistant columns have been traced as examples, but fabric can be seen across the entire outcrop and is particularly consistent in the lower portion of the image. Sol 3060 Mastcam mosaic mcam15984.

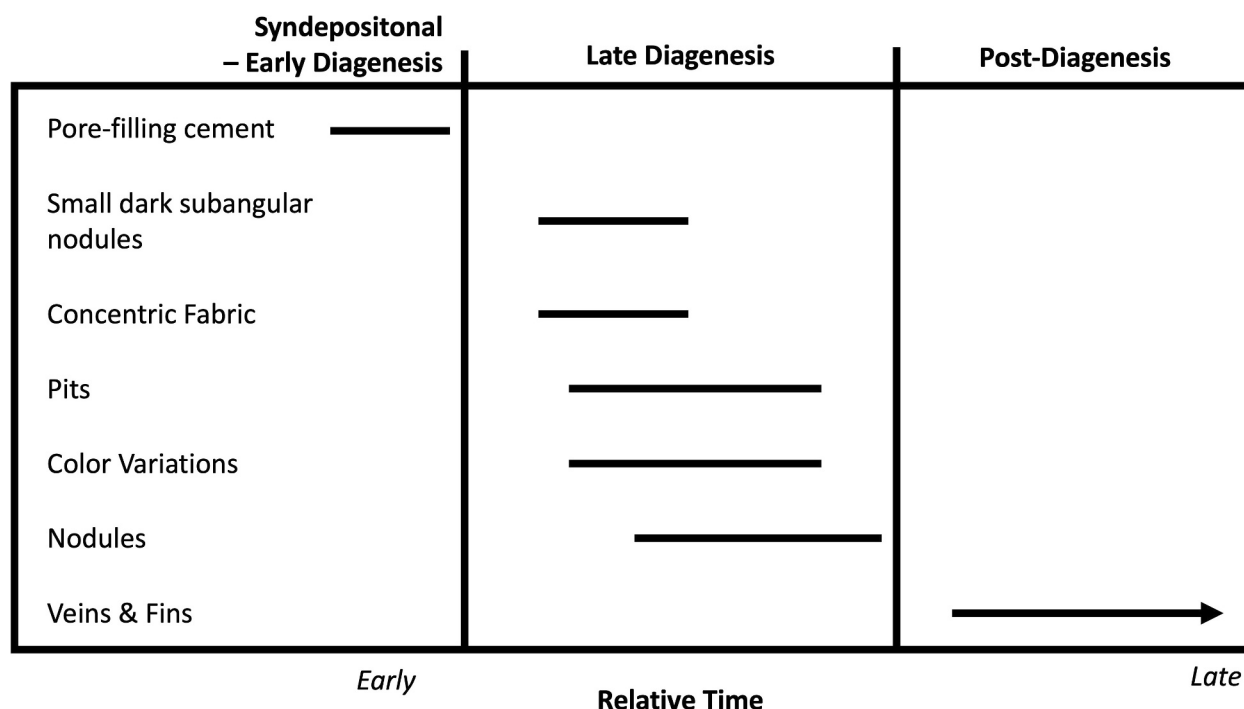
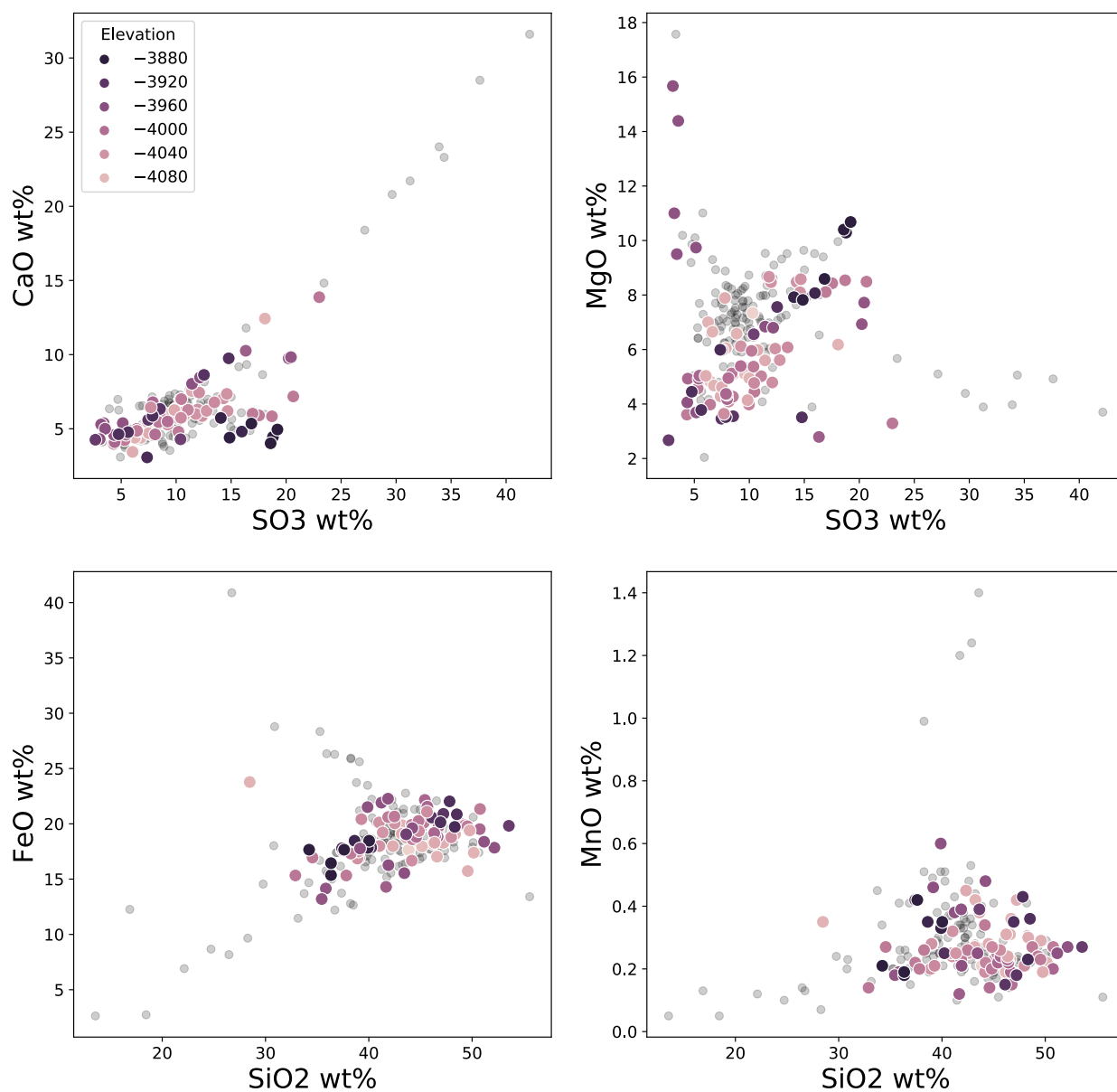


Figure 8. Schematic diagram showing the relative paragenetic sequence of diagenetic feature formation in relative time.

#### 5.4. Chemical Context

Previous work has demonstrated that Martian nodules can have similar or distinct chemical compositions as compared to their host rock (Gasda et al., 2022; Sun et al., 2019). Using ChemCam data, Meyer et al. (2024) demonstrate that the nodules in this region are enriched in sulfate (dominantly Mg, but some Fe as well), which may in part contribute to the orbital spectroscopic Mg sulfate signatures identified by Milliken et al. (2010) and Sheppard et al. (2021). CheMin drill data show that while the Nontron and Bardou drill holes bracketing Mont Mercou contain 18 wt.% and 12 wt.% nontronite, respectively, Pontours and Maria Gordon only have a trace amount of phyllosilicate, and Zechstein does not contain any above the CheMin detection limit of 1 wt.% (Rampe et al., 2022). The disappearance of clay minerals throughout the clay-sulfate transition region is not accompanied by an increase in Mg sulfate observed by CheMin (which did not detect any crystalline Mg sulfate until the Canaima drill target, as reported by Chipera et al., 2023), though the SAM instrument did detect small amounts of Mg sulfate in the latter three drill targets, suggesting that the Mg sulfate in this region is X-ray amorphous (Clark et al., 2023; Rampe et al., 2022). Observations by the MSL instrument suite therefore support the interpretation that the Mg sulfates of this region are amorphous products contained within the heterogeneously distributed diagenetic nodules. Thus, the “clay-sulfate transition” region is marked by a significant decline in clay minerals without a commensurate significant increase in the concentration of sulfate until the detection of crystalline Mg sulfate at the end of our study region.

Elemental composition may vary across specific parts of nodules, and also from nodule to nodule, as shown by ChemCam measurements of individual nodules (Meyer et al., 2024). It is therefore useful to accompany ChemCam measurements with APXS analyses, which can average intra- and inter-nodule heterogeneities within the instrument field of view. Elemental plots for nodular targets overlying all APXS targets within the study area demonstrate elemental enrichment in nodules in certain parts of the stratigraphy (Figure 9). Note that these trends reflect the overall nodular abundances measured for each outcrop, and do not account for the presence or absence of nodules in the center of the APXS field of view; deconvolving the spectrum to isolate nodule composition could further illuminate these trends but is outside the scope of this work. Nodules are the only diagenetic fabric element isolated for this data set because targets with most other feature types (veins, color variations, etc.) also contain nodules, making it impossible to compositionally isolate them with APXS. Given the abundance of certain elements in both terrestrial and Martian concretions (e.g., Gasda et al., 2022; Sun et al., 2019) we looked at



**Figure 9.** Elemental abundances for all APXS targets in the study area (light gray), with nodule-rich DRT targets highlighted with hue corresponding to elevation (as a proxy for stratigraphic position).

Mn, Fe, Si, Na, and Cl to try and understand what the cementing phase was that created differential resistance to weathering.

Mn is not enriched above the background within the nodular targets. However, plots of FeO versus SiO<sub>2</sub> display two distinct trends: bedrock targets (light gray points in Figure 9) have a population exhibiting a positive correlation, which may indicate the presence of detrital mafic minerals or clays like Fe/Mg smectites. In a second population, FeO and SiO<sub>2</sub> are anticorrelated, possibly reflecting an iron oxide enrichment consistent with CheMin detections of Fe oxides within the study region. The subpopulation of highlighted nodular targets falls along the positive correlation line with a weak but significant relationship ( $r^2 = 0.1086$ ), indicating that there may be a clay contribution to the nodule composition. Previous analyses of diagenetic fabrics earlier in the rover's traverse detected Mg-Fe phyllosilicates cementing raised ridges in the Sheepbed Mudstone (LeVeille et al., 2014); therefore, while the expression of features is different, the composition may have precedent.

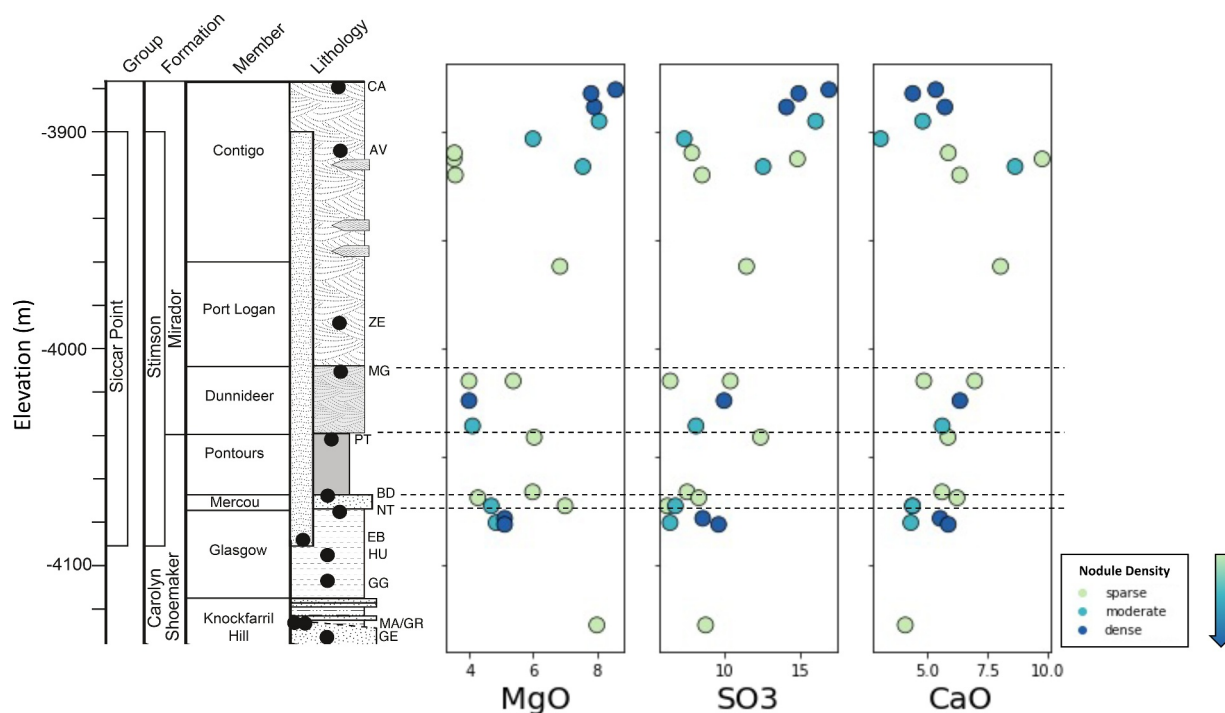


**Figure 10.** General correlations between quantitative nodule abundance classes and elemental enrichment in wt.% MgO, SO<sub>3</sub>, and CaO in APXS targets across the clay-sulfate transition.

The set of nodular targets closest to Canaima (therefore at the top of the stratigraphic section) fall close to the MgSO<sub>4</sub> addition line, while also showing significantly lower levels of CaO. Targets in the lower portion of the stratigraphic section also cluster around the MgSO<sub>4</sub> addition line, even when they are lower in Mg. These measurements corroborate the increased Mg sulfate detected in individual nodules by ChemCam (Meyer et al., 2024).

We also consider how nodules can contribute to the bulk rock elemental signature as measured by APXS by correlating their quantitative abundance to subtle changes in Mg, S, and Fe measurements (Berger, 2024). Nodule density measurements presented in Section 5.1 were correlated with the APXS elemental abundances for those same targets (Figure 10). While outcrops with all nodule densities can be found throughout the stratigraphic section, the densely nodular targets in the upper Mirador formation also tend to have the higher concentrations of both MgO and SO<sub>3</sub>, and lower enrichment in CaO. We can therefore use these measurements in conjunction with the ChemCam detections of Mg sulfate within certain nodules to infer that in the upper stratigraphy of the clay-sulfate transition region, amorphous Mg sulfate is concentrated in nodules and cement at such abundance that they influence the bulk rock elemental composition as measured by APXS.

## 6. Discussion

The chemical and morphological diversity of diagenetic fabrics in the study area indicate a complex set of paleohydrologic and diagenetic reaction events. Here, we explore possible formation mechanisms for these fabrics and textures, including early formation in either evaporite horizons or efflorescence from near-surface brines, or later formation due to precipitation from briny groundwater.

### 6.1. Hypothesis 1: Evaporitic Surface Crusts and Efflorescence

We first consider if nodule formation was dominantly the result of evaporitic concentration within shallow pools and near surface efflorescence to form salt-enriched sediments, perhaps associated with periods of wetting and drying. Such a process was first described in Gale crater by the Stein et al. (2018) analysis of desiccation cracks in the Old Soaker outcrop of the Murray formation. However, in that instance, no associated enrichment of salt was



observed, demonstrating that not all dry environments on Mars became briny environments. The raised polygonal ridges described in Section 4.5 have been interpreted to be similar evidence of desiccation features by Rapin et al. (2023). However, the raised ridges bounding the polygons are morphologically consistent with the larger amalgamated nodules across this entire area, and particularly similar to the other regularly spaced nodule patterns that are not necessarily indicative of desiccation processes (e.g., Figure 3e). The nodular texture of the fracture infill could indicate that deeply buried desiccation cracks created a zone of higher porosity and permeability that locally increased brine accumulation and subsequent nodule cementation. Therefore, these polygons could represent small isolated pools with wetting and drying processes but do not explain the breadth of diagenetic textures observed in this area, which also include isolated nodules and nodules grouped in linear formations and chevron patterns; here, we explore the spectrum of possible formation mechanisms that could complement the desiccation crack interpretation. It is perhaps likely that all of these organized textures—the polygons and the chevroned ridges, etc.—could reflect nucleation and reaction processes similar to Liesegang banding (Ortoleva, 1993) or diagenetic roll front mineralization (e.g., Granger & Warren, 1969) but precipitating sulfate cement. Nucleation and chemical precipitation on Earth may be biologically mediated, if not the direct replacement of bioclasts or encasing bioclasts (e.g., phosphate nodules in the Tégulines Clay, Lerouge et al., 2018). However, numerical and experimental models show that the complex patterns created by redox (and other) reactions can also be abiotic (e.g., Ortoleva, 1993) and with heterogeneity due to slight variations in pH or pore space permeability, it is reasonable for abiogenic nucleation on Mars to produce the patterns of nodules described here. Perhaps it is precisely because of the lack of microbial substrates to aid in nucleation that Mars produces the organized nodule patterns that may not have common terrestrial analogs.

Two different outcrops were also observed around Sol 3476 to have angular square nodules reminiscent in shape of halite hopper crystals, which could be pseudomorphs preserving evidence for primary or early diagenetic evaporites. However, these angular nodules are not confined to individual bedding planes and are not concentrated as abundantly as they are typically found in the terrestrial rock record (e.g., Gornitz & Schreiber, 1981). Should these be pseudomorphs after halite, we might expect to see NaCl enrichment in the surrounding rock; however, these outcrops do not correspond to the higher NaCl targets observed in the APXS data set. It would then be required that another episode of later fresher fluids leached out the salts.

These angular nodules are a unique morphology among the large database of nodules analyzed in this study area, and with the available data, our characterization as hopper-like is suggestive but not definitive. Therefore, they are not representative of the nodule features as a whole, and the interpretation that they may be evidence of primary evaporites cannot be extrapolated.

We also consider the possibility that the nodules formed early via efflorescence from near-surface brines. Terrestrial occurrences of starkeyite are usually produced by efflorescence; therefore, the detection of small amounts of crystalline starkeyite in the Canaima drill sample (Chipera et al., 2023) is the best indicator of this process of formation in near-surface layers during gradual drying. This is similar to the presence of starkeyite in Mesozoic sandstones along the Rio Puerco, NM (Szykiewicz et al., 2014). However, terrestrial examples of efflorescence form crusts on the surface rather than nodular horizons (and the nodules cataloged in this study are not confined to single beds but rather are distributed throughout the outcrops where they are observed). These crusts should produce draping layers over salt crusts or disruption to primary stratification, neither of which has been observed in the study area. Further, there are no sedimentary breccias or fracture networks reflecting surface layers collapsed over dissolved crust (e.g., Friedman, 1997). We would also expect to see accompanying features reflecting cyclical wetting and drying, such as teepee structures, desiccation cracks, or prism cracks (Allen, 1987; Assereto & Kendall, 1977), none of which are observed in the Canaima vicinity. The sediments of Gale crater, including the dune/interdune strata of the Mirador formation (Edgar et al., 2024), formed under long-term aggradational conditions; if primary, bedded evaporites formed and then eroded away, we would still expect to see evidence of their disruption to primary bedding or subsequent deposition (we do not). It is possible that there were lower evaporation rates on Mars—about 1 mm/yr modeled by Andrews-Hannah & Lewis (2011) as compared to 0.1 mm/day in the Chilean Altiplano (Johnson et al., 2010)—which could maintain an evaporating water table at a greater depth than on Earth, and the additional overburden pressure of a few meters of accumulating sediment would prevent these signature evaporitic sedimentary structures from forming. As there is no evidence to support the formation of salt crusts, it seems that another process may be required to explain the presence of the Starkeyite.

## 6.2. Hypothesis 2: Top-Down Dense Brines From Younger or Remobilized Sulfates

In all observed nodular outcrops, the nodules cross-cut bedding planes and are distributed throughout the rock. There are no examples of primary laminae truncated against nodules, bending under them, or draping on top of them. However, there are a small number of nodules with lamination preserved inside the nodule, indicating formation at a later time postdating compaction (e.g., Meyer et al., 2024, white arrows in Figure 9A and 9D). Given the smaller value of  $g$  on Mars, compaction would have taken place at greater depths in the crust of Mars as compared to Earth (Grotzinger et al., 2015), suggesting a deeper level for subsurface formation.

Late-stage concretions are abundant on Earth, and the iron oxide Moqui marbles eroding out of Jurassic Navajo sandstones serve as analogs for the spherical hematite-cemented “blueberries” discovered in Meridiani Planum (e.g., Chan et al., 2000; Chan et al., 2004). While these redox-driven concretions are not compositional analogs to the nodules in this study, they do provide good examples of late-stage fluid movement through porous rock, a process which was invoked by Sun et al. (2019) in their analysis of diagenetic concretions from lower in the Gale crater stratigraphy. It seems that late-stage concretion formation may be common on Mars, perhaps more so than early diagenetic concretions for which compelling analogs do not currently exist at any rover landing site.

Indeed, the concretions described here are nodules dominated by magnesium sulfate and not iron oxides. This complicates their understanding as late-stage diagenetic features formed during deeper burial. On Earth, magnesium sulfate concretions formed at depth are not observed, but secondary calcium sulfate precipitates are (Warren, 2016). Indiana carbonate sequences described by Maliva (1987) provide evidence that as dense brines sink, dolomitization releases Ca ions to form secondary anhydrite at depths of 30–40 m, and Machel (2013) found that more than 90% of anhydrite found in deeply buried (<1 km) Devonian carbonates of the Alberta Basin, Canada are replacive and may even postdate dolomitization. Deep brines can also be remobilized by groundwater fluids and reprecipitated in laterally adjacent strata; Rivera and Calderhead (2022) model groundwater migration in the Canadian Rockies, with deep (~1–2 km) brines transported hundreds of kilometers laterally toward the basin margin. Therefore, there is a terrestrial precedent for the movement and precipitation of secondary, non-“evaporite” sulfates at depth.

In one scenario, we propose a “top-down” hypothesis in which bedded evaporites deposited in stratigraphically higher units would have formed dense brines that would penetrate strata at lower elevations in the basin via gravitational drive. In particular, the evaporite source for those dense brines would be represented by the “boxwork” Mg sulfates—possibly evaporites—that occur at ~–3,500 m (Siebach & Grotzinger, 2014), though the “boxwork” composition cannot be known with certainty until the rover reaches the region (Figure 11a). Salinity increases during periods of drying to form the boxwork (or other, yet-unknown sulfate sources) could have produced dense brines that would have become gravitationally unstable, seeping downward through the underlying stratigraphy and precipitating in patches as concretions and cements within the study area. The distribution of nodules across the lower stratigraphy would then relate directly to permeability gradients across the mudstones and sandstones. An overall decrease in grain size moving downwards through the section from Canaima to Mary Anning, with a marked shift from sandstone to mudstone occurring within the Pontours member, is consistent with the greater concentration and diversity of nodules at these stratigraphic levels. Meyer et al. (2024) propose that a basal Mirador formation unconformity could provide the rapid grain size change and pathways needed to produce the observed zone of intense nodular overprinting in the Pontours member, with fluids concentrated in this member due to clay in the underlying stratigraphy. Indeed, the higher clay content present in the Carolyn Shoemaker formation (Glen Torridon region) below our study area, which decreases at Mont Mercou and disappears in the upper parts of stratigraphy (except, perhaps, in the form of Mg-Fe phyllosilicates in the nodules), could have formed an aquitard at the base of this section. Our results complement the Meyer et al. (2024) ChemCam-based nodule analysis, and we further suggest that the diversity and abundance of diagenetic textures concentrated just below Mont Mercou captured in the MAHLI data set are consistent with the porosity and permeability gradients in the stratigraphy. In this scenario, the Mg sulfates in the Mirador formation at –4,000 m would be roughly the same age as the putative “boxwork” sulfates at –3,500 m since they derive from a fluid source that was generated during deposition of the Mt. Sharp group. This timing of diagenesis could also contribute to the abundance of x-ray amorphous material throughout the not-yet lithified Murray formation via destabilization of clay minerals by silica-poor brines, and is consistent with the “top down” model presented in both Bristow et al. (2021) and Meyer et al. (2024).

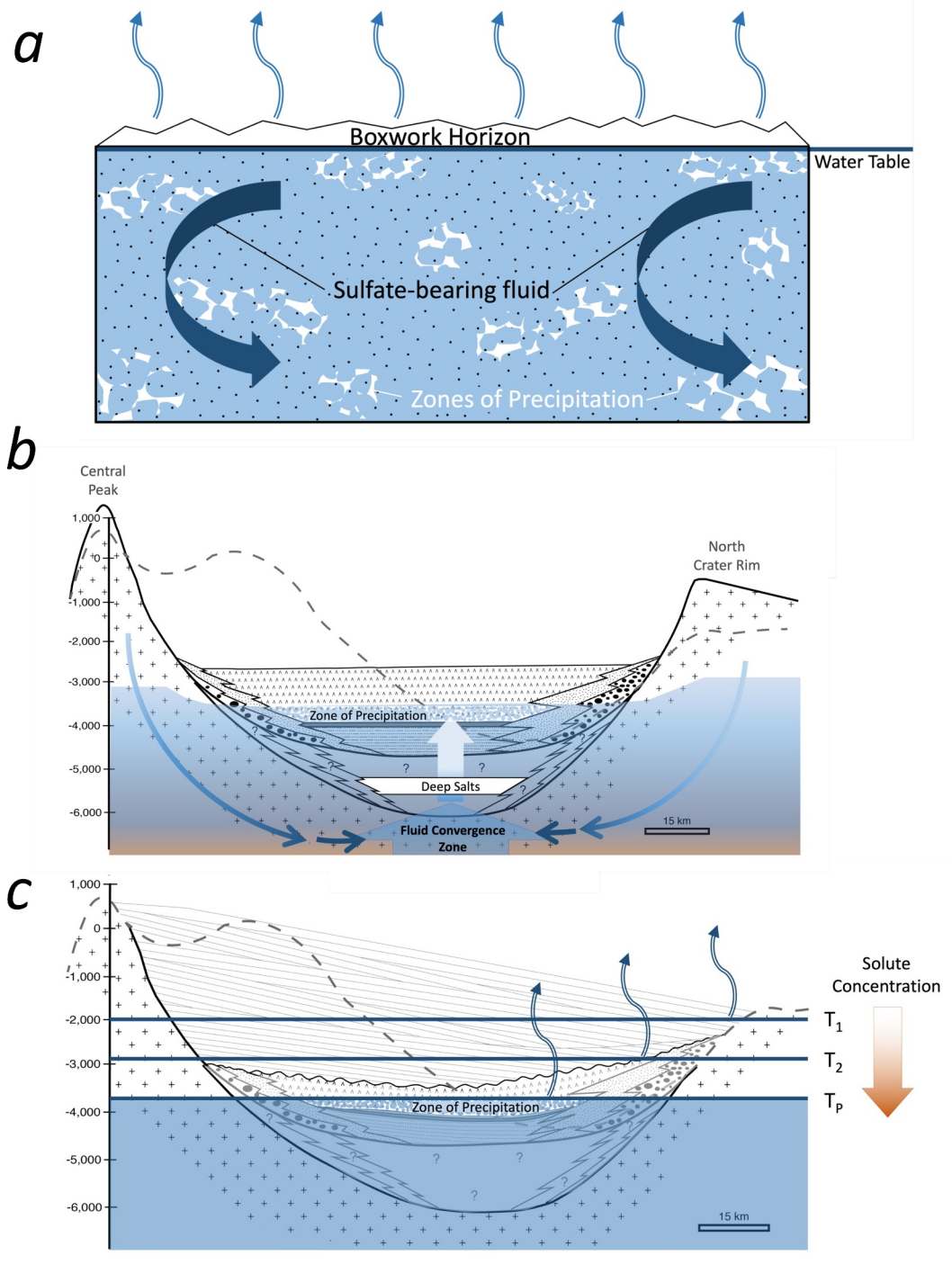


Figure 11.

A variant of this scenario, also involving gravitational drive, is that the “boxwork” or other higher Mg sulfates could have been remobilized by post-Mt. Sharp group fluids, perhaps associated with the incision of Gediz Vallis to penetrate through older rocks via fracture and matrix porosity. Hurowitz et al. (2017) proposed that the layered “boxwork” sulfates (~–3,500 m) observed at higher elevations in Mt. Sharp group strata could have been remobilized during younger fluid flow, with gravity-driven penetration of dense brines to precipitate in topographically lower but stratigraphically younger rocks of the Stimson formation. In this scenario, the Mg sulfates in the Mirador formation would be much younger than the Mt. Sharp group “boxwork” Mg sulfates. This age difference could be on the order of ~ billion years as Martin et al. (2021) showed by dating jarosite in the Mt. Sharp group that was markedly younger than the age of the Mt. Sharp group strata (Murray formation) that hosts these sulfate minerals.

### 6.3. Hypothesis 3: Bottom-Up Precipitation From Deep Groundwater Brines

A third distinct hypothesis would involve remobilization of salts buried in the crater at a depth below Curiosity's landing elevation (Figure 11b). The depth of the infill beneath the rover could reach 1.5 km based on estimates of the crater impact topography (Grotzinger et al., 2015) and it is possible that early fill included evaporites as well as detrital sediments derived from the crater wall and central peak. These brines could have formed in situ or been transported laterally, perhaps several hundreds of kilometers, from the large recharge area to the south of Gale crater, which serves as a regional low point (e.g., Andrews-Hanna et al., 2012; Zolotov & Mironenko, 2016). The presence of these deep brines could indicate regional or even global fluctuations in early Mars climate history to first emplace and then later circulate the sulfate. The strong hydraulic gradient coming down from the crater rim, where meteoric waters enter the crater, and the weaker gradient coming from the taller but spatially restricted central peak would meet and mix in the subsurface. Residual heat generated from the crater-forming impact or the ambient geothermal gradient could have provided the necessary heat input to drive the mixed fluids upwards through the stratigraphy; Schwenzer et al. (2012) demonstrated that an impact-driven hydrothermal system could have persisted in the bottom of Gale crater for several hundred thousand years, and the geothermal gradient could contribute to fluid movement for the millions of years timescales of Mount Sharp deposition. The resulting upwelling of groundwater through a buried evaporite deposit would dissolve Mg sulfate and carry the ions upwards in solution due to thermal buoyancy. Mg sulfate solubility increases with temperature, and even a slight decrease in temperature from a mostly cooled hydrothermal system to the colder strata above would decrease the solubility of Mg sulfate (Krumgalz, 2018). The decrease in pressure ascending through several km of vertical strata (perhaps on the order of ~50 bar/km) would also contribute to reduced solubility, though to a lesser degree than temperature, following well-studied solubility-pressure relationships in Ca sulfates on Earth (e.g., Blount & Dickson, 1973). Gradual evaporation of near-surface water would slowly increase the concentration of Mg sulfate until a threshold is reached and precipitation is triggered by the changing physical-chemical conditions; in a deeper groundwater scenario where a fluid was supersaturated at depth and cooled as it rose, pore spaces could serve as nucleation points for rapid crystallization. Slight local variations in porosity and permeability of the sediments could result in a heterogeneous distribution of Mg sulfate cements, as reflected in the spatial heterogeneity of nodules documented in this study. This model would require the movement of deep waters through low-porosity, impermeable layers, such as Glen Torridon, but the heavily fractured outcrops observed in Glen Torridon could be evidence of fracture-conduits allowing the upward passage of Mg-rich fluids. These proposed mechanisms incorporate elements of processes observed on Earth, but the terrestrial record lacks a direct analog;

**Figure 11.** Schematic illustration of hypothesized processes for Mg sulfate precipitation in nodular bedrock, modified from Grotzinger et al. (2015) Figure 8. (a) Hypothesis 2: Top-down fluid migration and diagenesis. Fluids originate as evaporative brines, here represented as boxwork formation at –3,500 m MOLA elevation (though they could come from other yet-unknown evaporite sources). These fluids are dense and descend via gravitational drive into the subsurface to the stratigraphic level of the Mirador formation (–4,000 m MOLA elevation) circulating and precipitating in the pore spaces within local patches above less permeable clay-bearing and finer-grained Glen Torridon sediments. This schematic represents one phase of a process that may have occurred several times as the groundwater system varied with sedimentation and aridity. (b) Hypothesis 3: Bottom-up fluid migration and diagenesis. Meteoric precipitation above the crater highlands infiltrates and is driven gravitationally to substantial depths in the buried crater sediments. This groundwater mixes with warmer fluids originating at depth as connate or hydrothermal fluids and rises up due to thermal warming, encountering sulfate evaporites from an early time in Gale's infilling. These remobilized sulfates may be leached to create brines that precipitate out at the top of the groundwater table to form patches of Mg-sulfate bearing strata in the Mirador formation. (c) Hypothesis 4: As Mars steadily desiccates due to the loss of the atmosphere, connate fluids in equilibrium with basaltic sediments evaporate in the subsurface. These fluids draw down to progressively greater depths and steadily increase their salt content to a level where Mg-sulfate precipitates in the pore space.

the Martian stratigraphic history may record a unique process in large-scale Mg sulfate remobilization and sedimentation.

#### 6.4. Hypothesis 4: Top-Down Precipitation Due To Desiccation of Mars

A final hypothesis centers around the well-established observation that Mars has lost a lot of its atmosphere and water to space (e.g., Jakosky & Phillips, 2001). This process was well underway by the time that the Gale crater began to fill with sediments (Mahaffy et al., 2015). The inevitable consequence is that surface water would evaporate and after that groundwater would evaporate. In that latter case, evaporation would be controlled by the aridity of the atmosphere and the permeability (diffusivity) of the sediments (or fractured bedrock). As time passed, the groundwater would diffuse through the sediments and into the atmosphere, the water table would be lowered, and any soluble salts would be concentrated to the point where they might precipitate as pore-filling cements (Figure 11c).

In a sedimentary basin like Gale crater, the groundwater would equilibrate with buried sediments so that solute composition would reflect sediment composition. Given the overwhelming concentration of basaltic sediments, it would be natural to expect these fluids to record that composition; elements such as magnesium and sulfur would be readily available, along with a host of other salts that could be concentrated to the point of precipitation (Tosca et al., 2005). Therefore, the observation of Mg sulfates in the strata of the Mirador formation could record this long-term desiccation of Mars.

### 7. Conclusions

There is a wide range of diversity and abundance in the expression of the diagenetic textures that have been observed along Curiosity's traverse to date, but they exhibit particularly diagnostic behavior throughout the clay-sulfate transition region. By cataloging all diagenetic textures observed in MAHLI images, including their abundances, morphologies, and relationships to each other, we find that changing abundance and diversity of textures parallels changes in stratigraphy, reflecting underlying fluid pathways. By analyzing cross-cutting relationships between the different feature types, we suggest a paragenetic sequence in which there are multiple phases of diagenetic fluid flow: at least two events are required to form co-occurring color variations, pits, and nodules, and to differentiate co-occurring populations of small and large, clustered nodules; two additional later stage events precipitated Ca sulfate veins, first in low-angle fractures nearly parallel to bedding, and later in high angle fractures (consistent with other examples of late-stage fracture-filling veins previously identified in the rover mission).

The Pontours member records strong overprinting diagenesis followed by an upward transition to pockets of nodules coincident with the transition between a fluvial-lacustrine to an aeolian depositional environment. Porosity and permeability differences controlled by aeolian sediment sorting processes may have focused subsurface flow along these better sorted sediments; perhaps the underlying sediments were less permeable due to their higher clay content, forcing fluids to migrate preferentially within the parts of the aquifer marked by the basal aeolian sediments of the Mirador formation. The phyllosilicate-rich sediments of the underlying Glen Torridon region may therefore have acted as an aquiclude, resulting in a twofold representation in the diagenetic record: the diversity of textures is extremely high within the laminated mudstones of the upper Glasgow member, perhaps due to increased circulation aided by interspersed coarser grained fluvial barforms like Mont Mercou just above the less permeable clay-rich lower Glasgow member, and the destruction of primary stratigraphy throughout the Pontours member, which may therefore be a zone of high porosity and permeability like the sandstones overlying it. The distinct outcrop-scale patterns (linear, polygonal, and chevroned ridges) formed by diagenetic nodules in the Pontours member may also reflect the movement of reaction fronts through the subsurface within the parts of the aquifer with higher hydraulic conductivity.

Correlating the quantitative abundance of nodules with subtle variations in APXS bulk rock chemistry—that is, densely nodular targets in the upper Contigo member correlate with MgO and SO<sub>3</sub> enrichment and CaO reduction—expands previous observations of Mg and Fe sulfate enrichment in individual nodules as well as bedrock, particularly in the upper part of the stratigraphic section. The apparent upward increase in nodule and cement contribution to bulk rock elemental composition through the section supports the hypothesis that these Mg sulfates were formed from small amounts of groundwater either dissolving salts in an overlying sulfate unit and transporting them downwards in dense brines or upwelling through deeply buried salts below. Though there is

some evidence for localized evaporite features, the lack of salt crystals, clear pseudomorphs, or disruption to primary lamination from draping or drying structures anywhere in the study region the requires alternative precipitation mechanisms, such as the movement of Mg sulfate from an over- or underlying unit, to explain the presence of these sulfates in the stratigraphy. The proposed hypotheses have implications for the global Mars climate, with the bottom-up model allowing for more longstanding circulation of recharged groundwater and the top-down models relating to the terminal aridification of Mars.

Overall, the morphology and diversity of diagenetic overprints in this key stratigraphic section of Gale crater, as lacustrine sediments give way to aeolian and surface water begins to dry, record at least four distinct episodes of diagenetic alteration. The distribution of these textures reflects the ease of fluid circulation through sediments overlying the less permeable clay-rich Glen Torridon region, and the Mg sulfate rich composition of nodules in the upper portions of the stratigraphic section records the late-stage movement of dense brines saturated with Mg sulfate sourced from elsewhere in the stratigraphy.

### Data Availability Statement

Data presented in this work are archived and freely available to the public in the NASA Planetary Data System (PDS): all APXS data (Berger, 2024; Gellert, 2013), Mastcam images (Malin, 2013), and MAHLI images (Edgett, 2013a, 2013b) used in this work are available in the PDS Geoscience Node and PDS Imaging Node. A list of all MAHLI observations used in this study with their accompanying characterization (presence/absence of all diagenetic textures as well as nodule classification) is available at the CaltechDATA site (Seeger & Grotzinger, 2024).

### Acknowledgments

We would like to thank the scientists and engineers of the MSL team, especially the Mastcam, MAHLI, and APXS payload uplink and downlink leads, for their work in obtaining the observations necessary for this study and diligent contributions towards mission success. Mastcam mosaics were processed by the Mastcam team at Malin Space Science Systems.

### References

- Allen, J. R. L. (1987). Desiccation of mud in the temperate intertidal zone: Studies from the Severn Estuary and eastern England. *Philosophical Transactions of the Royal Society of London B Biological Sciences*, 315(1171), 127–156. <https://doi.org/10.1098/rstb.1987.0005>
- Anderson, R., & Bell III, J. F. (2010). Geologic mapping and characterization of Gale Crater and implications for its potential as a Mars Science Laboratory landing site. *MARS J.*, 5, 76–128.
- Andrews-Hanna, J. C., & Lewis, K. W. (2011). Early Mars hydrology: 2. Hydrological evolution in the Noachian and Hesperian epochs. *Journal of Geophysical Research*, 116(E2), E02007. <https://doi.org/10.1029/2010JE003709>
- Andrews-Hanna, J. C., Soto, A., & Richardson, M. I. (2012). The hydrologic and climatic context of the Gale crater sedimentary mound. *Third Conference on Early Mars: Hydrologic, and Climatic Evolution and the Implications for Life*, 1680, 7038.
- Assereto, R., & Kendall, C. (1977). Nature, origin and classification of peritidal tepee structures and related breccias. *Sedimentology*, 24(2), 153–210. <https://doi.org/10.1111/j.1365-3091.1977.tb00254.x>
- Banner, J. L., & Hanson, G. N. (1990). Calculation of simultaneous isotopic and trace element variations during water-rock interaction with applications to carbonate diagenesis. *Geochimica et Cosmochimica Acta*, 54(11), 3123–3137. [https://doi.org/10.1016/0016-7037\(90\)90128-8](https://doi.org/10.1016/0016-7037(90)90128-8)
- Beitler, B., Chan, M. A., & Parry, W. T. (2003). Bleaching of Jurassic Navajo Sandstone on Colorado Plateau Laramide highs: Evidence of exhumed hydrocarbon supergiants? *Geology*, 31(12), 1041–1044. <https://doi.org/10.1130/G19794.1>
- Beitler, B., Parry, W. T., & Chan, M. A. (2005). Fingerprints of fluid flow: Chemical diagenetic history of the Jurassic Navajo Sandstone, southern Utah, USA. *Journal of Sedimentary Research*, 75(4), 547–561. <https://doi.org/10.2110/jsr.2005.045>
- Bell III, J. F., Godber, A., McNair, S., Caplinger, M. A., Maki, J. N., Lemmon, M. T., et al. (2017). The Mars Science Laboratory Curiosity rover Mastcam instruments: Preflight and in-flight calibration, validation, and data archiving. *Earth and Space Science*, 4(7), 396–452. <https://doi.org/10.1002/2016EA000219>
- Berger, J. A. (2024). Elemental composition and geological context of MSL APXS targets from sol 3054 to 3712 [Dataset]. *PDS Geosciences Node*. <https://doi.org/10.17189/1139-2w66>
- Blake, D., Vaniman, D., Achilles, C., Anderson, R., Bish, D., Bristow, T., et al. (2012). Characterization and calibration of the CheMin mineralogical instrument on Mars Science Laboratory. *Space Science Reviews*, 170(1–4), 341–399. <https://doi.org/10.1007/s11214-012-9905-1>
- Blount, C. W., & Dickson, F. W. (1973). Gypsum-anhydrite equilibria in systems CaSO<sub>4</sub>-H<sub>2</sub>O and CaCO<sub>4</sub>-NaCl-H<sub>2</sub>O. *American Mineralogist: Journal of Earth and Planetary Materials*, 58(3–4\_Part\_1), 323–331.
- Bowen, B., Martini, B. A., Chan, M. A., & Parry, W. T. (2007). Reflectance spectroscopic mapping of diagenetic heterogeneities and fluid-flow pathways in the Jurassic Navajo Sandstone. *AAPG Bulletin*, 91(2), 173–190. <https://doi.org/10.1306/08220605175>
- Bristow, T. F., Grotzinger, J. P., Rampe, E. B., Cuadros, J., Chipera, S. J., Downs, G. W., et al. (2021). Brine-driven destruction of clay minerals in Gale crater, Mars. *Science*, 373(6551), 198–204. <https://doi.org/10.1126/science.abg5449>
- Campbell, J. L., Perrett, G. M., Gellert, R., Andrusenko, S. M., Boyd, N. I., Maxwell, J. A., et al. (2012). Calibration of the Mars Science Laboratory alpha particle X-ray spectrometer. *Space Science Reviews*, 170(1), 319–340. <https://doi.org/10.1007/s11214-012-9873-5>
- Caravaca, G., Mangold, N., Dehouck, E., Schieber, J., Zaugg, L., Bryk, A. B., et al. (2022). From lake to river: Documenting an environmental transition across the Jura/Knockfarril Hill members boundary in the Glen Torridon region of Gale crater (Mars). *Journal of Geophysical Research: Planets*, 127(9), e2021JE007093. <https://doi.org/10.1029/2021JE007093>
- Cardenas, B. T., Grotzinger, J. P., Lamb, M. P., Lewis, K. W., Fedo, C. M., Bryk, A. B., et al. (2022). Barform deposits of the Carolyn Shoemaker formation, Gale crater, Mars. *Journal of Sedimentary Research*, 92(12), 1071–1092. <https://doi.org/10.2110/jsr.2022.032>
- Caswell, T. E., & Milliken, R. E. (2017). Evidence for hydraulic fracturing at Gale crater, Mars: Implications for burial depth of the Yellowknife Bay formation. *Earth and Planetary Science Letters*, 468, 72–84. <https://doi.org/10.1016/j.epsl.2017.03.033>

- Chan, M. A., Beitler, B., Parry, W. T., Ormó, J., & Komatsu, G. (2004). A possible terrestrial analogue for haematite concretions on Mars. *Nature*, 429(6993), 731–734. <https://doi.org/10.1038/nature02600>
- Chan, M. A., Bowen, B. B., Parry, W., Ormó, J., & Komatsu, G. (2005). Red rock and red planet diagenesis. *Geological Society of America Today*, 15, 4–10.
- Chan, M. A., Parry, W. T., & Bowman, J. R. (2000). Diagenetic hematite and manganese oxides and fault-related fluid flow in Jurassic sandstones, southeastern Utah. *AAPG Bulletin*, 84(9), 1281–1310. <https://doi.org/10.1306/A9673E82-1738-11D7-8645000102C1865D>
- Chipera, S. J., Vaniman, D. T., Rampe, E. B., Bristow, T. F., Martínez, G., Tu, V. M., et al. (2023). Mineralogical investigation of Mg-sulfate at the Canaima drill site, Gale Crater, Mars. *Journal of Geophysical Research: Planets*, 128(11), e2023JE008041. <https://doi.org/10.1029/2023JE008041>
- Clark, J. V., Sutter, B., Lewis, J., Mcadam, A. C., Archer, P. D., Franz, H., et al. (2023). Mineralogical and chemical changes in the clay-sulfate transition region as detected by the sample analysis at Mars-evolved gas analyzer (SAM-EGA) in Gale Crater, Mars. In *54th lunar and planetary science conference*.
- Downs, R. T., & MSL Science Team. (2015). Determining mineralogy on Mars with the CheMin X-ray diffractometer. *Elements*, 11(1), 45–50. <https://doi.org/10.2113/gselements.11.1.45>
- Edgar, L., Grotzinger, J., Fedo, C. M., Meyer, M., Rapin, W., Dietrich, W. E., et al. (2024). Wet to dry depositional environments recorded in the clay-sulfate transition region in Gale Crater, Mars: Overview and stratigraphic context for curiosity's exploration campaign. In *55th lunar and planetary science conference* (p. 1016).
- Edgett, K. S. (2013a). MSL MARS HAND LENS IMAGER 2 EDR IMAGE V1.0 [Dataset]. *NASA Planetary Data System*. <https://doi.org/10.17189/1520187>
- Edgett, K. S. (2013b). MSL MARS HAND LENS IMAGER 2 EDR ZSTACK V1.0 [Dataset]. *NASA Planetary Data System*. <https://doi.org/10.17189/1520396>
- Edgett, K. S., Yingst, R. A., Ravine, M. A., Caplinger, M. A., Maki, J. N., Ghaemi, F. T., et al. (2012). Curiosity's Mars hand lens imager (MAHLI) investigation. *Space Science Reviews*, 170(1–4), 259–317. <https://doi.org/10.1007/s11214-012-9910-4>
- Fedo, C. M., Bryk, A. B., Edgar, L. A., Bennett, K. A., Fox, V. K., Dietrich, W. E., et al. (2022). Geology and stratigraphic correlation of the Murray and Carolyn Shoemaker formations across the Glen Torridon region, Gale crater, Mars. *Journal of Geophysical Research: Planets*, 127(9), e2022JE007408. <https://doi.org/10.1029/2022JE007408>
- Fraeman, A. A., Arvidson, R. E., Catalano, J. G., Grotzinger, J. P., Morris, R. V., Murchie, S. L., et al. (2013). A hematite-bearing layer in Gale Crater, Mars: Mapping and implications for past aqueous conditions. *Geology*, 41(10), 1103–1106. <https://doi.org/10.1130/G34613.1>
- Fraeman, A. A., Edgar, L. A., Rampe, E. B., Thompson, L. M., Frydenvang, J., Fedo, C. M., et al. (2020). Evidence for a diagenetic origin of Vera Rubin ridge, Gale crater, Mars: Summary and synthesis of Curiosity's exploration campaign. *Journal of Geophysical Research: Planets*, 125(12), e2020JE006527. <https://doi.org/10.1029/2020JE006527>
- Friedman, G. M. (1997). Dissolution-collapse breccias and paleokarst resulting from dissolution of evaporite rocks, especially sulfates. *Carbonates and Evaporites*, 12(1), 53–63. <https://doi.org/10.1007/BF03175802>
- Frydenvang, J., Gasda, P. J., Hurowitz, J. A., Grotzinger, J. P., Wiens, R. C., Newsom, H. E., et al. (2017). Diagenetic silica enrichment and late-stage groundwater activity in Gale crater, Mars. *Geophysical Research Letters*, 44(10), 4716–4724. <https://doi.org/10.1002/2017GL073323>
- Gasda, P. J., Comellas, J., Essunfeld, A., Das, D., Bryk, A. B., Dehouck, E., et al. (2022). Overview of the morphology and chemistry of diagenetic features in the clay-rich Glen Torridon unit of Gale crater, Mars. *Journal of Geophysical Research: Planets*, 127(12), e2021JE007097. <https://doi.org/10.1029/2021JE007097>
- Gellert, R. (2013). MSL Mars alpha particle X-ray spectrometer 4/5 RDR V1.0 [Dataset]. *NASA Planetary Data System*. <https://doi.org/10.17189/1518757>
- Gornitz, V. M., & Schreiber, B. C. (1981). Displacive halite hoppers from the Dead Sea; some implications for ancient evaporite deposits. *Journal of Sedimentary Research*, 51(3), 787–794. <https://doi.org/10.1306/212F7DAB-2B24-11D7-8648000102C1865D>
- Granger, H. C., & Warren, C. G. (1969). Unstable sulfur compounds and the origin of roll-type uranium deposits. *Economic Geology*, 64(2), 160–171. <https://doi.org/10.2113/gsecongeo.64.2.160>
- Grotzinger, J. P., Arvidson, R. E., Bell III, J. F., Calvin, W., Clark, B. C., Fike, D. A., et al. (2005). Stratigraphy and sedimentology of a dry to wet eolian depositional system, Burns formation, Meridiani Planum, Mars. *Earth and Planetary Science Letters*, 240(1), 11–72. <https://doi.org/10.1016/j.epsl.2005.09.039>
- Grotzinger, J. P., Gupta, S., Malin, M. C., Rubin, D. M., Schieber, J., Siebach, K., et al. (2015). Deposition, exhumation, and paleoclimate of an ancient lake deposit, Gale crater, Mars. *Science*, 350(6257), aac7575. <https://doi.org/10.1126/science.aac7575>
- Grotzinger, J. P., Sumner, D. Y., Kah, L. C., Stack, K., Gupta, S., Edgar, L., et al. (2014). A habitable fluvio-lacustrine environment at Yellowknife Bay, Gale crater, Mars. *Science*, 343(6169), 1242777. <https://doi.org/10.1126/science.1242777>
- Hurowitz, J. A., Grotzinger, J. P., Fischer, W. W., McLennan, S. M., Milliken, R. E., Stein, N., et al. (2017). Redox stratification of an ancient lake in Gale crater, Mars. *Science*, 356(6341), eaah6849. <https://doi.org/10.1126/science.aah6849>
- Inagaki, F., Hinrichs, K. U., Kubo, Y., Bowles, M. W., Heuer, V. B., Hong, W. L., et al. (2015). Exploring deep microbial life in coal-bearing sediment down to ~ 2.5 km below the ocean floor. *Science*, 349(6246), 420–424. <https://doi.org/10.1126/science.aaa6882>
- Jakosky, B. M., & Phillips, R. J. (2001). Mars' volatile and climate history. *Nature*, 412(6843), 237–244. <https://doi.org/10.1038/35084184>
- Johnson, E., Yáñez, J., Ortiz, C., & Muñoz, J. (2010). Evaporation from shallow groundwater in closed basins in the Chilean Altiplano. *Hydrological Sciences Journal—Journal des Sciences Hydrologiques*, 55(4), 624–635. <https://doi.org/10.1080/02626661003780458>
- Kah, L. C., Stack, K. M., Eigenbrode, J. L., Yingst, R. A., & Edgett, K. S. (2018). Syndepositional precipitation of calcium sulfate in Gale Crater, Mars. *Terra Nova*, 30(6), 431–439. <https://doi.org/10.1111/ter.12359>
- Knoll, A. H., & Grotzinger, J. (2006). Water on Mars and the prospect of Martian life. *Elements*, 2(3), 169–173. <https://doi.org/10.2113/gselements.2.3.169>
- Kronyak, R. E., Kah, L. C., Edgett, K. S., VanBommel, S. J., Thompson, L. M., Wiens, R. C., et al. (2019). Mineral-filled fractures as indicators of multigenerational fluid flow in the Pahrump Hills member of the Murray formation, Gale crater, Mars. *Earth and Space Science*, 6(2), 238–265. <https://doi.org/10.1029/2018EA000482>
- Krumgalz, B. S. (2018). Temperature dependence of mineral solubility in water. Part 3. Alkaline and alkaline earth sulfates. *Journal of Physical and Chemical Reference Data*, 47(2). <https://doi.org/10.1063/1.5031951>
- Le Deit, L., Hauber, E., Fueten, F., Pondrelli, M., Rossi, A. P., & Jaumann, R. (2013). Sequence of infilling events in Gale Crater, Mars: Results from morphology, stratigraphy, and mineralogy. *Journal of Geophysical Research: Planets*, 118(12), 2439–2473. <https://doi.org/10.1002/2012JE004322>
- Lerouge, C., Robinet, J. C., Debure, M., Tournassat, C., Bouchet, A., Fernández, A. M., et al. (2018). A deep alteration and oxidation profile in a shallow clay aquitard: Example of the Tégulines Clay, East Paris Basin, France. *Geofluids*, 2018, 1–20. <https://doi.org/10.1155/2018/1606753>

- Léveillé, R. J., Bridges, J., Wiens, R. C., Mangold, N., Cousin, A., Lanza, N., et al. (2014). Chemistry of fracture-filling raised ridges in Yelowknife Bay, Gale Crater: Window into past aqueous activity and habitability on Mars. *Journal of Geophysical Research: Planets*, 119(11), 2398–2415. <https://doi.org/10.1002/2014JE004620>
- L'Haridon, J., Mangold, N., Meslin, P. Y., Johnson, J. R., Rapin, W., Forni, O., et al. (2018). Chemical variability in mineralized veins observed by ChemCam on the lower slopes of Mount Sharp in Gale crater, Mars. *Icarus*, 311, 69–86. <https://doi.org/10.1016/j.icarus.2018.01.028>
- Machel, H. G. (2013). Secondary anhydrites in deeply buried Devonian carbonates of the Alberta Basin, Canada. *Carbonates and Evaporites*, 28(3), 267–280. <https://doi.org/10.1007/s13146-012-0123-4>
- Magnabosco, C., Lin, L.-H., Dong, H., Bomberg, M., Ghiorse, W., Stan-Lotter, H., et al. (2018). The biomass and biodiversity of the continental subsurface. *Nature Geoscience*, 11(10), 707–717. <https://doi.org/10.1038/s41561-018-0221-6>
- Mahaffy, P. R., Webster, C. R., Stern, J. C., Brunner, A. E., Atreya, S. K., MSL Science Team, et al. (2015). The imprint of atmospheric evolution in the D/H of Hesperian clay minerals on Mars. *Science*, 347(6220), 412–414. <https://doi.org/10.1126/science.1260291>
- Malin, M. C. (2013). MSL MARS MAST CAMERA 2 EDR IMAGE V1.0 [Dataset]. *NASA Planetary Data System*. <https://doi.org/10.17189/1520190>
- Malin, M. C., & Edgett, K. S. (2000). Sedimentary rocks of early Mars. *Science*, 290(5498), 1927–1937. <https://doi.org/10.1126/science.290.5498.1927>
- Malin, M. C., Ravine, M. A., Caplinger, M. A., Tony Ghaemi, F., Schaffner, J. A., Maki, J. N., et al. (2017). The Mars Science Laboratory (MSL) mast cameras and descent imager: Investigation and instrument descriptions. *Earth and Space Science*, 4(8), 506–539. <https://doi.org/10.1002/2016EA000252>
- Maliva, R. G. (1987). Quartz geodes; early diagenetic silicified anhydrite nodules related to dolomitization. *Journal of Sedimentary Research*, 57(6), 1054–1059. <https://doi.org/10.1306/212F8CE7-2B24-11D7-8648000102C1865D>
- Martin, P. E., Farley, K. A., Malespin, C. A., Mahaffy, P. R., Edgett, K. S., Gupta, S., et al. (2021). Billion-year exposure ages in Gale crater (Mars) indicate Mount Sharp formed before the Amazonian period. *Earth and Planetary Science Letters*, 554, 116667. <https://doi.org/10.1016/j.epsl.2020.116667>
- McLennan, S. M., Bell III, J. F., Calvin, W. M., Christensen, P. R., Clark, B. D., De Souza, P. A., et al. (2005). Provenance and diagenesis of the evaporite-bearing Burns formation, Meridiani Planum, Mars. *Earth and Planetary Science Letters*, 240(1), 95–121. <https://doi.org/10.1016/j.epsl.2005.09.041>
- McLennan, S. M., Grotzinger, J. P., Hurowitz, J. A., & Tosca, N. J. (2019). The sedimentary cycle on early Mars. *Annual Review of Earth and Planetary Sciences*, 47(1), 91–118. <https://doi.org/10.1146/annurev-earth-053018-060332>
- Meyer, M. J., Milliken, R. E., Stack, K. M., Edgar, L. A., Rampe, E. B., Turner, M. L., et al. (2024). The geological context and significance of the clay-sulfate transition region in Mount Sharp, Gale Crater, Mars: An integrated assessment based on orbiter and rover data. *GSA Bulletin*.
- Milliken, R. E., Grotzinger, J. P., & Thomson, B. J. (2010). Paleoclimate of Mars as captured by the stratigraphic record in Gale Crater. *Geophysical Research Letters*, 37(4), L04201. <https://doi.org/10.1029/2009GL041870>
- Mondro, C. A., Grotzinger, J. P., Fedo, C. M., & Paar, G. (2023). Fracture patterns in Mont Mercou record changing stress fields during burial and exhumation of Mount Sharp, Gale Crater, Mars. *Geological Society of America Abstracts with Programs*, 55(6), 391634. <https://doi.org/10.1130/abs/2023AM-391634>
- Moser, D. P., Gihring, T., Fredrickson, J. K., Brockman, F. J., Balkwill, D., Dollhopf, M. E., et al. (2005). Desulfotomaculum spp. and Methanobacterium spp. dominate 4–5 km deep fault. *Applied and Environmental Microbiology*, 71(12), 8773–8783. <https://doi.org/10.1128/AEM.71.12.8773-8783.2005>
- Nachon, M., Clegg, S. M., Mangold, N., Schröder, S., Kah, L. C., Dromart, G., et al. (2014). Calcium sulfate veins characterized by ChemCam/Curiosity at Gale crater, Mars. *Journal of Geophysical Research*, 119(9), 1991–2016. <https://doi.org/10.1002/2013JE004588>
- Nachon, M., Mangold, N., Forni, O., Kah, L. C., Cousin, A., Wiens, R. C., et al. (2017). Chemistry of diagenetic features analyzed by ChemCam at Pahrump Hills, Gale crater, Mars. *Icarus*, 281, 121–136. <https://doi.org/10.1016/j.icarus.2016.08.026>
- Onstott, T. C., Ehlmann, B. L., Sapers, H., Coleman, M., Ivarsson, M., Marlow, J. J., et al. (2019). Paleo-rock-hosted life on Earth and the search on Mars: A review and strategy for exploration. *Astrobiology*, 19(10), 1230–1262. <https://doi.org/10.1089/ast.2018.1960>
- Ortoleva, P. (1993). Geochemical self-organization. *Oxford Monographs on Geology and Geophysics*.
- Parry, W. T., Chan, M. A., & Beitle, B. (2004). Chemical bleaching indicates episodes of fluid flow in deformation bands in sandstone. *AAPG Bulletin*, 88(2), 175–191. <https://doi.org/10.1306/09090303034>
- Potter, S. L., Chan, M. A., Petersen, E. U., Dyar, M. D., & Sklute, E. (2011). Characterization of Navajo Sandstone concretions: Mars comparison and criteria for distinguishing diagenetic origins. *Earth and Planetary Science Letters*, 301(3–4), 444–456. <https://doi.org/10.1016/j.epsl.2010.11.027>
- Rampe, E. B., Bristow, T. F., Blake, D. F., Vaniman, D. T., Chipera, S. J., Downs, R. T., et al. (2022). Mineralogical trends over the clay-sulfate transition in Gale Crater from the Mars Science Laboratory CheMin instrument. In *53rd Lunar and Planetary science conference*.
- Rampe, E. B., Ming, D. W., Blake, D. F., Bristow, T. F., Chipera, S. J., Grotzinger, J. P., et al. (2017). Mineralogy of an ancient lacustrine mudstone succession from the Murray formation, Gale crater, Mars. *Earth and Planetary Science Letters*, 471, 172–185. <https://doi.org/10.1016/j.epsl.2017.04.021>
- Rapin, W., Dromart, G., Clark, B. C., Schieber, J., Kite, E. S., Kah, L. C., et al. (2023). Sustained wet–dry cycling on early Mars. *Nature*, 620(7973), 299–302. <https://doi.org/10.1038/s41586-023-06220-3>
- Rivera, A., & Calderhead, A. I. (2022). Glacial melt in the Canadian Rockies and potential effects on groundwater in the plains region. *Water*, 14(5), 733. <https://doi.org/10.3390/w14050733>
- Rivera-Hernández, F., Sumner, D. Y., Mangold, N., Banham, S. G., Edgett, K. S., Fedo, C. M., et al. (2020). Grain size variations in the Murray formation: Stratigraphic evidence for changing depositional environments in Gale crater, Mars. *Journal of Geophysical Research: Planets*, 125(2), e2019JE006230. <https://doi.org/10.1029/2019JE006230>
- Schwenzer, S. P., Abramov, O., Allen, C. C., Bridges, J. C., Clifford, S. M., Filiberto, J., et al. (2012). Gale Crater: Formation and post-impact hydrous environments. *Planetary and Space Science*, 70(1), 84–95. <https://doi.org/10.1016/j.pss.2012.05.014>
- Seeger, C., & Grotzinger, J. P. (2024). Diagenesis of the clay-sulfate stratigraphic transition, Mount Sharp Group, Gale Crater, Mars [Dataset]. *CaltechDATA*. <https://doi.org/10.22002/krdbt-e4j31>
- Seiler, W. M. (2008). *Jurassic Navajo Sandstone of Coyote Buttes, Utah/Arizona: Coloration and diagenetic history, preservation of a dinosaur trample surface, and a terrestrial analog to Mars. Doctoral dissertation*. the University of Utah.
- Sheppard, R. Y., Milliken, R. E., Parente, M., & Itoh, Y. (2021). Updated perspectives and hypotheses on the mineralogy of lower Mt. Sharp, Mars, as seen from orbit. *Journal of Geophysical Research: Planets*, 126(2), e2020JE006372. <https://doi.org/10.1029/2020JE006372>
- Siebach, K. L., & Grotzinger, J. P. (2014). Volumetric estimates of ancient water on Mount Sharp based on boxwork deposits, Gale Crater, Mars. *Journal of Geophysical Research: Planets*, 119(1), 189–198. <https://doi.org/10.1002/2013JE004508>



- Siebach, K. L., Grotzinger, J. P., Kah, L. C., Stack, K. M., Malin, M., Léveillé, R., & Sumner, D. Y. (2014). Subaqueous shrinkage cracks in the Sheepbed mudstone: Implications for early fluid diagenesis, Gale crater, Mars. *Journal of Geophysical Research*, *119*(7), 1597–1613. <https://doi.org/10.1002/2014JE004623>
- Squyres, S. W., Grotzinger, J. P., Arvidson, R. E., Bell III, J. F., Calvin, W., Christensen, P. R., et al. (2004). In situ evidence for an ancient aqueous environment at Meridiani Planum, Mars. *Science*, *306*(5702), 1709–1714. <https://doi.org/10.1126/science.1104559>
- Stack, K. M., Grotzinger, J. P., Kah, L. C., Schmidt, M. E., Mangold, N., Edgett, K. S., et al. (2014). Diagenetic origin of nodules in the Sheepbed member, Yellowknife Bay formation, Gale crater, Mars. *Journal of Geophysical Research*, *119*(7), 1637–1664. <https://doi.org/10.1002/2014JE004617>
- Stein, N., Grotzinger, J. P., Schieber, J., Mangold, N., Hallet, B., Newsom, H., et al. (2018). Desiccation cracks provide evidence of lake drying on Mars, Sutton Island member, Murray formation, Gale Crater. *Geology*, *46*(6), 515–518. <https://doi.org/10.1130/G40005.1>
- Sumner, N. S., & Verosub, K. L. (1992). Diagenesis and organic maturation of sedimentary rocks under volcanic strata, Oregon. *AAPG Bulletin*, *76*(8), 1190–1199. <https://doi.org/10.1306/bdff89a2-1718-11d7-8645000102c1865d>
- Sun, V. Z., Stack, K. M., Kah, L. C., Thompson, L., Fischer, W., Williams, A. J., et al. (2019). Late-stage diagenetic concretions in the Murray formation, Gale crater, Mars. *Icarus*, *321*, 866–890. <https://doi.org/10.1016/j.icarus.2018.12.030>
- Szynkiewicz, A., Borrok, D. M., & Vaniman, D. T. (2014). Efflorescence as a source of hydrated sulfate minerals in valley settings on Mars. *Earth and Planetary Science Letters*, *393*, 14–25. <https://doi.org/10.1016/j.epsl.2014.02.035>
- Thomson, B. J., Bridges, N. T., Milliken, R., Baldrige, A., Hook, S. J., Crowley, J. K., et al. (2011). Constraints on the origin and evolution of the layered mound in Gale Crater, Mars using Mars Reconnaissance Orbiter data. *Icarus*, *214*(2), 413–432. <https://doi.org/10.1016/j.icarus.2011.05.002>
- Tice, M. M., & Lowe, D. R. (2004). Photosynthetic microbial mats in the 3,416-Myr-old ocean. *Nature*, *431*(7008), 549–552. <https://doi.org/10.1038/nature02888>
- Tosca, N. J., Knoll, A. H., & McLennan, S. M. (2008). Water activity and the challenge for life on early Mars. *Science*, *320*(5880), 1204–1207. <https://doi.org/10.1126/science.1155432>
- Tosca, N. J., McLennan, S. M., Clark, B. C., Grotzinger, J. P., Hurowitz, J. A., Knoll, A. H., et al. (2005). Geochemical modeling of evaporation processes on Mars: Insight from the sedimentary record at Meridiani Planum. *Earth and Planetary Science Letters*, *240*(1), 122–148. <https://doi.org/10.1016/j.epsl.2005.09.042>
- Treiman, A. H., Lanza, N. L., VanBommel, S., Berger, J., Wiens, R., Bristow, T., et al. (2023). Manganese-iron phosphate nodules at the Groken Site, Gale Crater, Mars. *Minerals*, *13*(9), 1122. <https://doi.org/10.3390/min13091122>
- VanBommel, S. J., Berger, J. A., Gellert, R., O'Connell-Cooper, C. D., McCraig, M. A., Thompson, L. M., et al. (2023). Elemental composition of manganese- and phosphorus-rich nodules in the Knockfarril Hill member, Gale crater, Mars. *Icarus*, *392*, 115372. <https://doi.org/10.1016/j.icarus.2022.115372>
- VanBommel, S. J., Gellert, R., Berger, J. A., Campbell, J. L., Thompson, L. M., Edgett, K. S., et al. (2016). Deconvolution of distinct lithology chemistry through oversampling with the Mars Science Laboratory alpha particle X-ray spectrometer. *X-Ray Spectrometry*, *45*(3), 155–161. <https://doi.org/10.1002/xrs.2681>
- VanBommel, S. J., Gellert, R., Berger, J. A., Thompson, L. M., Edgett, K. S., McBride, M. J., et al. (2017). Modeling and mitigation of sample relief effects applied to chemistry measurements by the Mars Science Laboratory Alpha Particle X-ray Spectrometer. *X-Ray Spectrometry*, *46*(4), 229–236. <https://doi.org/10.1002/xrs.2755>
- Warren, J. K. (2016). *Evaporites: A geological compendium*. Springer.
- Wiens, R. C., Maurice, S., Barraclough, B., Saccoccio, M., Barkley, W. C., Bell, J. F., III, et al. (2012). The ChemCam instrument suite on the Mars Science Laboratory (MSL) rover: Body unit and combined system tests. *Space Science Reviews*, *170*(1–4), 167–227. <https://doi.org/10.1007/s11214-012-9902-4>
- Wiens, R. C., Rubin, D. M., Goetz, W., Fairen, A. G., Schwenzer, S. P., Johnson, J. R., et al. (2017). Centimeter to decimeter hollow concretions and voids in Gale Crater sediments, Mars. *Icarus*, *289*, 144–156. <https://doi.org/10.1016/j.icarus.2017.02.003>
- Williams, R. M., Grotzinger, J. P., Dietrich, W. E., Gupta, S., Sumner, D. Y., Wiens, R. C., et al. (2013). Martian fluvial conglomerates at Gale crater. *Science*, *340*(6136), 1068–1072. <https://doi.org/10.1126/science.1237317>
- Yen, A. S., Ming, D. W., Vaniman, D. T., Gellert, R., Blake, D. F., MSL Science Team, et al. (2017). Multiple stages of aqueous alteration along fractures in mudstone and sandstone strata in Gale Crater, Mars. *Earth and Planetary Science Letters*, *471*, 186–198. <https://doi.org/10.1016/j.epsl.2017.04.033>
- Zolotov, M. Y., & Mironenko, M. V. (2016). Chemical models for martian weathering profiles: Insights into formation of layered phyllosilicate and sulfate deposits. *Icarus*, *275*, 203–220. <https://doi.org/10.1016/j.icarus.2016.04.011>